Cosmic muon magnetic moment and lifetime.

v1.4

Matei A.V. Climescu

Mainz, 2021

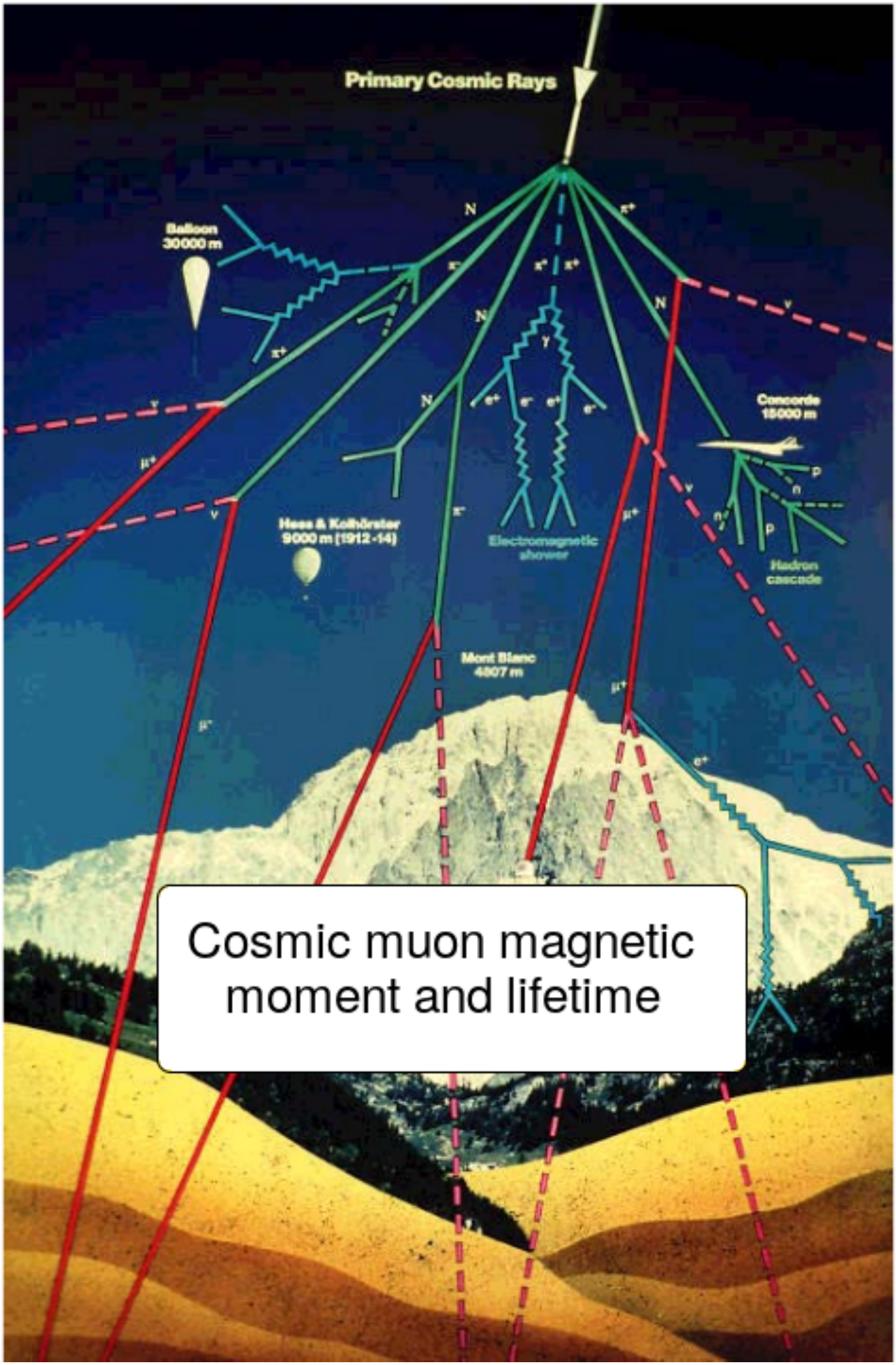

Cosmic muon magnetic moment and lifetime

Chapter 1

Introduction

This experiment is based on the Diplomarbeit of Mathias Heel in 1982 (*Aufbau eines Versuchs im Fortgeschrittenen-Praktikum zur Messung der Lebendauer von Myonen*) and in particular the Staatsexamensarbeit of Joachim Geisbüsch in 1991 (Verbesserungen zum Experiment) at the University of Mainz's Departement of Physics. This experiment script was re-written in English by Matei Climescu in 2020 from Andreas Winhart's German version from 2001. The full latex source is publicly available at https://github.com/matclim/muonlifetime for improvements, updates and changes, it is generally advised that students also look at the repository to ensure they have the latest version.

This experiment allows for the determination of the lifetime and magnetic moment of cosmic muons. Students can have a first introduction to elementary particle physics measurements and analysis methods with relatively simple means.

The muon μ^- is an elementary particle often referred to as the electron's 'heavy cousin'. It has identical properties to the electron and thus behaves in the same way, if the electron's mass was 207 times larger. The same can be said for the charged tau lepton τ^- (sometimes called the tauon) albeit with a 3491 mass factor instead. This gives rise to the concept of Lepton universality. The reason why the number of lepton generations is three remains unclear. Muons are of particular interest because:

- Parity violation in the weak sector is a particularly important part of modern physics: nature isn't invariant to spatial transformations, this is one of the results of the experiment.
- A fairly accurate measurement for the weak coupling constant can be performed along with the muon's lifetime. The measurement of the anomalous magnetic moment of the muon, the so-called 'g-2 factor' is an important test for the validity of QED.
- Muons are the main component of sea-level cosmic radiation. The radiation density remains low however: the verticle flux of muons above 1 GeV/c

Chapter 2

The Standard Model of Particle Physics

Over the past few decades, elementary particle physics has known a string of unprecedented progress, this was notably linked to the rise of the Standard Model which itself was notably propelled by the closer study of cosmic rays, radiation naturally falling from the sky. Closer investigation of cosmic radiation yielded the discovery of many new particles, such as neutral Kaons K^0 in 1947, prompting Nobel prize Willis Lamb to declare "The finder of a new elementary particle used to be rewarded by a Nobel Prize, but such a discovery now ought to be punished by a 10,000 dollar fine.", expressing the difficulty felt by the theoreticians of the time to make sense of the situation. As new techniques, such as particle accelerators, were improved, this 'Particle Zoo' became even more confusing to physicists. In the 1960s and 70s, a new model emerged: the Standard Model which sought to bring order to this apparent chaos. It did so by articulating the phenomenology of known fundamental interactions into a single self-consistent, locally gauge-invariant quantum field theory centered around electromagnetism (Quantum Electro-Dynamics or *QED*), the strong nuclear force (Quantum Chromo-Dynamics or *QCD*) and the weak nuclear force.

Those interactions are mediated by spin-1 particles, the so-called *vector-bosons*: the photon γ mediates QED, eight massless but coloured gluons g mediate QCD and three massive bosons Z, $\mathrm{W}^{\pm}$ mediate the weak interaction. Finally a single spinless massive *scalar boson*, the so-called *Higgs Boson* was observed in 2012 and allows for massive bosons and at least certain fermions to be massive. All those bosons can be found in Table 2.2. Each interaction takes place via the exchange of its bosons, for example, the β^- decay of ^{137}Cs to ^{137}Ba can in fact be seen as a neutron's d emitting a W^- and thus becoming a u, causing the neutron to become a proton. This reaction can be seen in Figure 2.1. Matter however is made of fermions, particles with spin $\frac{1}{2}$, those, in the Standard Model are classified as *quarks* and *leptons*. The Standard Model was observed to hold 6 massive quarks, reacting to all three interactions, 3 charged leptons, sensitive to electromagnetism and the weak interaction, and 3 neutral leptons, *neutrinos*, which only interact through the weak interaction. They can be found in Table 2.1.

Generation	**1**		**2**		**3**	
	Fermion	Mass [MeV]	Fermion	Mass [MeV]	Fermion	Mass [MeV]
Up-type quarks ($q = 2/3$)	up (u)	~ 2.2	charm (c)	~ 1300	top (t)	173000
Down-type quarks ($q = -1/3$)	down (d)	~ 4.7	strange (s)	~ 95	beauty/bottom (b)	~ 4200
Charged leptons ($q = -1$)	electron (e^-)	0.511	muon (μ^-)	113	tau (τ^-)	1780
Neutrinos ($q = 0$)	electron neutrino (ν_e)	~ 0	muon neutrino (ν_μ)	~ 0	tau neutrino (ν_τ)	~ 0

Table 2.1: Standard Model fermions.

Ordinary matter is overwhelmingly composed of first generation particles: *up* and *down* quarks and *electrons*, a proton is notably composed of two up-type quarks and one down-type quark while a neutron is composed of a single up-type quark and two down-type quarks. It should be noticed that this is mostly due to the unstable nature of particles from Generation 2 and 3 (with the notable exception of neutrinos). Those particles will decay into lighter ones, as a general rule, heavier

Interaction	Boson	Mass [GeV]	Range [m]	Time scale [s]	spin	coupling	Fields
Strong	gluon (g)	0	10^{-15}	10^{-23}	1	~ 1	Quarks
Electromagnetic	photon (γ)	0	inf	10^{-20}	1	1/137	Electric charge
Weak	Z-zero boson (Z^0), W bosons ($W^{\pm}$)	91.2, 80.4	~ 10^{-17}	10^{-8}	1	10^{-5}	Quarks and leptons
Higgs	boson H	125.2	~ 10^{-18}	~ 10^{-22}	0	variable	Massive fields
Gravity	graviton (g)	0	inf	-	2	> 10^{-41}	Massive fields

Table 2.2: Standard Model force carriers.

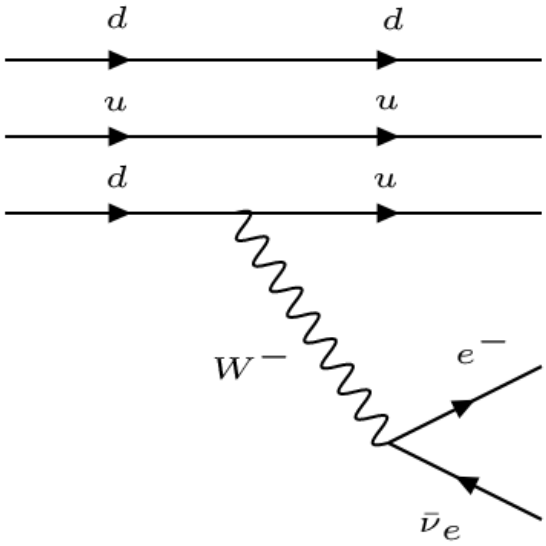

Figure 2.1: Weak decay of a neutron to a proton.

particles decay faster and thus have a shorter lifetime.

Chapter 3

Cosmic Radiation

3.1 History of cosmic radiation

In 1785, Charles-Augustin de Coulomb discovered that charge was released by a charged electroscope over time. Over a century later, Wilson and Geitel discovered ionization currents using a bell apparatus shown in Figure 3.1. They noticed that a dark current persisted in the bell and that, despite it being weakened by covering the apparatus in lead, it could never quite be eliminated, leading them to postulate the existence of telluric radioactivity (or Earth radioactivity).

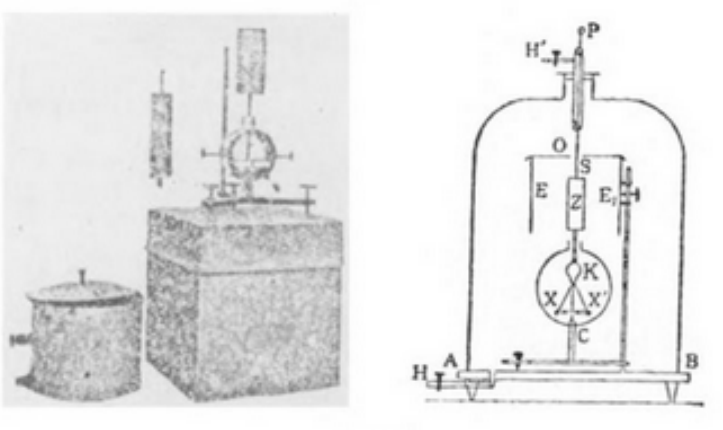

Figure 3.1: Geitel's ionization current apparatus (1900).

It wasn't until 1912 that it was determined that the source of this "dark current" couldn't be the earth: Victor Hess experimented with putting an electroscope onto a balloon which he launched to an altitude of up to 5300 m. He found that the rate of radiation was there some three times what it was at sea level and this, allied with his experimentation during a partial solar eclipse, allowed him to rule out the Sun as the source of this myterious radiation, enabling him to discover a natural source of high-energy particles: cosmic rays, awarding him the Nobel prize in 1936. Later studies from Freier, Lofgren, Ney, Oppenheimer, Bradt and Peters from 1948 and many others accross the years showed the existence of different radiation in the upper atmosphere, the so-called primary radiation, composed of around 90% protons and around 10% other nuclei which corresponds to the material ratio found in your average star, leading to the conclusion that cosmic radiation was mostly emitted by stars.

3.2 Primary cosmic rays

In star explosions, such as Supernovae, electric fields arise at the star's surface, this implies the acceleration of charged particles to very high energies. Particles thus gain enough energy to exit the star's potential well but whether they actually are able to be emitted is also dependent on their mass: lighter particles such as e^- see their energy quickly depleted through *bremsstrahlung emissions*. This is due to the way the emitted bremsstrahlung energy E_{Brems} evolves relative to the emitting particle's mass m_{P}:

$$E_{\text{Brems}} \propto \frac{1}{m_{\text{P}}^2}. \tag{3.1}$$

This implies that protons and heavy nuclei are the main constituents of what exits the star.

When this primary radiation enters the atmosphere, it's deflected by the Earth's B-field via the Lorentz force. At our latitude (50°-Mainz Gutenbergplatz), particles require at least 3 GeV to enter the atmosphere. This values varies around the globe and is in particular lower near the poles since there is a higher proportion of field lines parralel to the Earth's surface. This is often called the *magnetic latitude effect* shown in Figure 3.2.

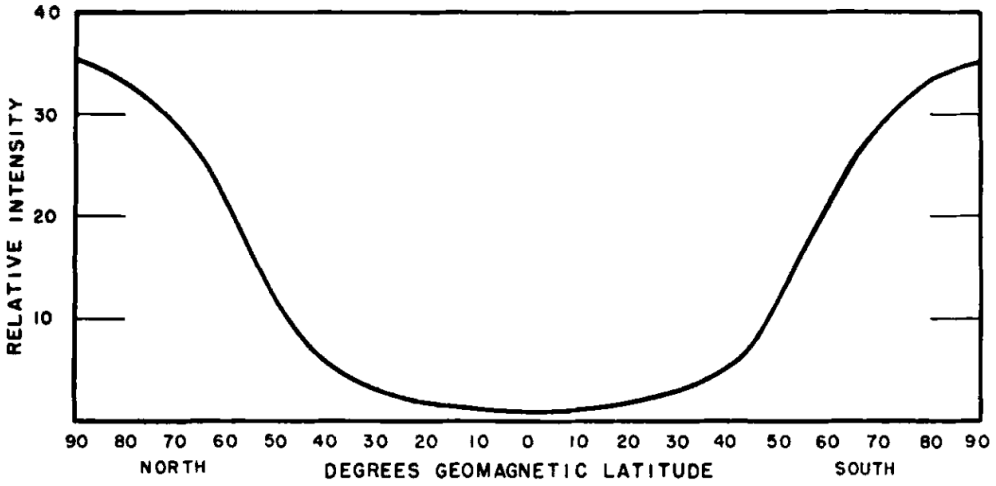

Figure 3.2: Magnetic latitude effect at sea level.

The Earth's **B**-field is a dipole field with magnetic moment of $8.1 \cdot 10^{18}$ J.G^{-1}. The critical momentum, the minimal momentum needed to breach the atmosphere is given by:

$$\mathrm{P}_{\Phi} = 1.5 \cdot 10^{10} \cos^4 \Phi |z| \text{ eV}.c^{-1}. \tag{3.2}$$

where z is the particle's charge in units of elementary charge. The discrenpency in the number of positive and negative particles results in an east-west asymmetry in particle intensity. At least 90% of the primary particles have a positive charge as shown in Figure 3.3.

3.3 Secondary comic rays

Since the atmosphere is a matter-rich environment, it provides any entering primary radiation with fields to interact with, which gives rise to a variety of processes, producing so-called *secondary cosmic rays*. Low energy protons, with momenta up to 10 GeV knock-off individual nucleons from nitrogen and oxygen nuclei. At higher energy, nuclear (meson-dominated) bremsstrahlung radiation is the main source of energy loss. An example of it can be found in Figure 3.4.

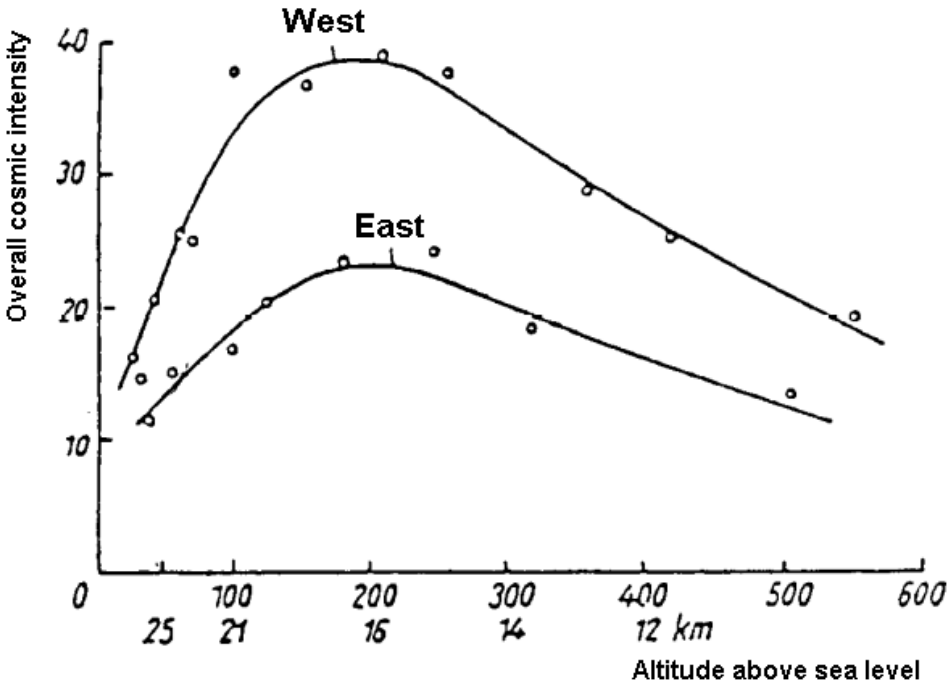

Figure 3.3: East-west asymmetry measured at different altitudes.

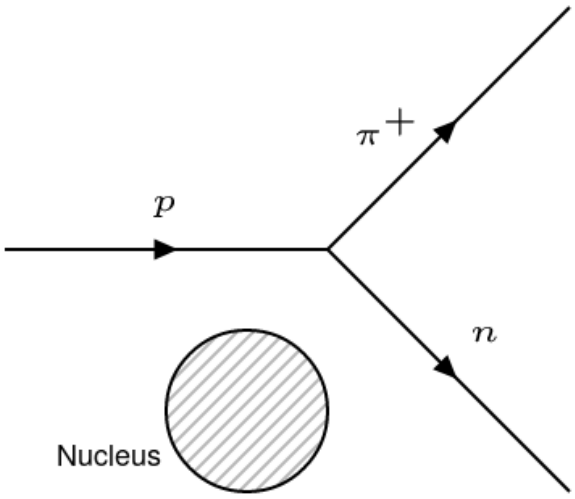

Figure 3.4: Bremsstrahlung pion emission from proton-nucleus scattering.

The produced mesons are mostly pions but heavier flavour particles can be created at energies above 100 GeV such as Kaons.

Protons from primary cosmic rays have an energy up to a couple PeV and will thus also perform nucleon-antinucleon pairs. This energy level remains very rare however as can be seen in Figure 3.5

The number N of protons for a given energy is given by:

$$\mathrm{N}(E) = K \cdot E^{-\gamma}.$$

where K is a constant and γ varies with the energy: from $\gamma = 1$ for $E = 10\,\mathrm{GeV}$ to $\gamma = 2.5$ for very high energies [8].

For our purpose, pions are of particular interest. Charged pions decay overwhelmingly (~ 99.99%) into a muon and a muon neutrino with a lifetime of $2.6 \cdot 10^{-8}$ s [8]:

$$\pi^+ \to \mu^+ + \nu_\mu \text{ and } \pi^- \to \mu^- + \overline{\nu}_\mu.$$

Because of their relatively low energy loss and long lifetimes, nearly all muons reach the Earth's surface.

3.4 Cosmic radiation content

There are three main components to cosmic radiation: so-called *hard-radiation*, *soft-radiation* and *nuclear-radiation*. A sketch of cosmic radiation and it's content can be found in Figure 3.6.

3.4.1 Nuclear radiation

As its name implies, nucleons and light atomic nuclei make up nuclear cosmic radiation. Atomic nuclei lose energy through absorption into the air while low energy protons lose theirs through ionization. Neutrons interact abundently with atmospheric nuclei through elastic scattering which creates a gain in thermal energy in said nuclei. The proportion of nuclear radiation reaching the earth's surface is negligible.

3.4.2 Soft radiation

γ and $\mathrm{e}^\pm$ are the constituents of soft cosmic radiation. Electrons arise partially from muon decays but mostly from photon pair creation. Those are mostly produced in two ways: electromagnetic bremsstrahlung/Cherenkov radiation and from the decay of neutral pions π^0. Neutral pions are produced as part of nuclear cosmic radiation and decay into photon pairs with a $8.52 \cdot 10^{-17}$ s lifetime [8]. Said photons will overwhelmingly decay into $\mathrm{e}^\pm$ pairs if they have an energy $E > 2m_\mathrm{e}$.

$$\pi^0 \to \gamma\gamma,\ \gamma \to \mathrm{e}^+\mathrm{e}^-,\ \mathrm{e}^\pm \to \mathrm{e}^\pm\gamma,\ \gamma \to \mathrm{e}^+\mathrm{e}^- \text{ etc..}$$

The pion's energy will thus be distributed over many particles until a so-called *critical energy* is reached. Under said energy, ionization, as opposed to particle creation, becomes the dominant energy loss mechanism which signals the end of the shower as the number of particles will thus quickly decrease. γ lose energy through the Compton and photoelectric effects which implies that those remaining particles can easily be shielded by a couple centimetres of lead.

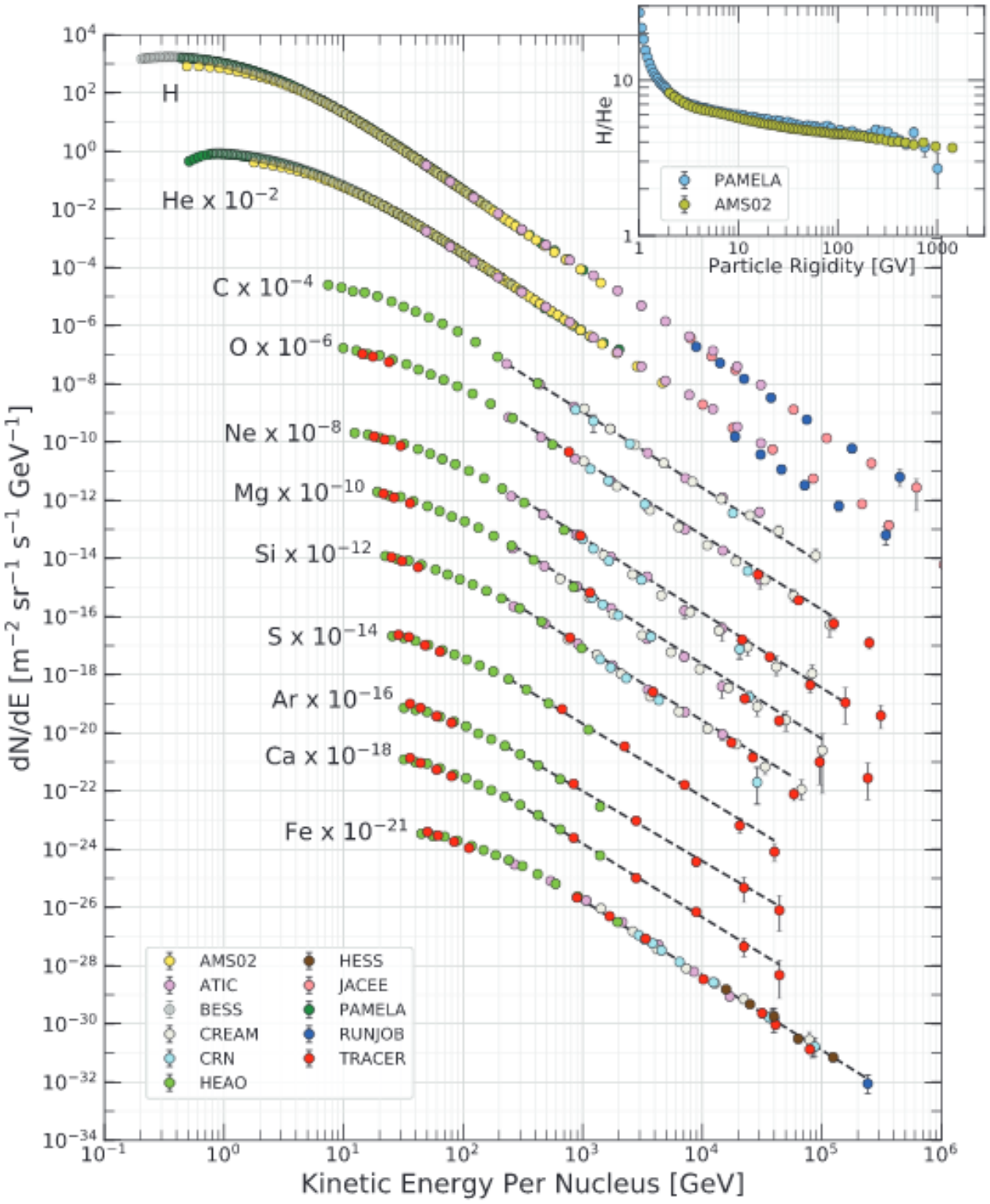

Figure 3.5: Fluxes of nuclei of the primary cosmic radiation in particles per-energy-per-nucleus are plotted vs energy-per-nucleus. The inset shows the H/He ratio at constant rigidity [8].

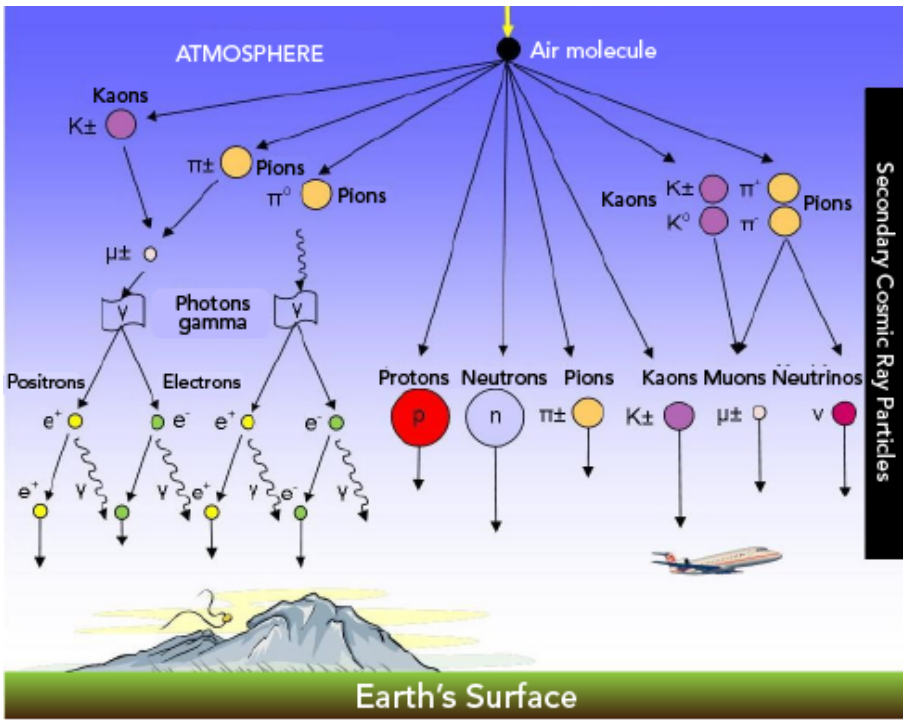

Figure 3.6: Cosmic rays and their components. On the left is the soft component, in the middle is the nuclear component and on the right is the hard component [7].

3.4.3 Hard radiation

The hard radiation component is revolves around heavy flavour leptons, mainly μ flavour ones. Due to their relatively high mass, muons only lose small amounts of energy due to bremsstrahlung and mostly through ionization since they have a very high critical energy ($\sim 3.6\,\mathrm{TeV}$). The energy loss of massive charged particles is described by the *Bethe-Bloch Formula*:

$$-\frac{\mathrm{d}E}{\mathrm{d}x} = \frac{4\pi n z^2 e^4}{m_\mathrm{e}}\left(\ln\left(\frac{2m_\mathrm{e}v^2}{I(1-\beta^2)} - \beta^2\right)\right). \tag{3.3}$$

where E is the energy, x the distance, n is the number of electrons per cm^3 in the traversed material, $z \cdot e$ is the electrical charge and v the particle's speed, I is the mean excitation potential of an atom in the material, often approximated by $I \simeq 17.7Z^{0.85}$ and β is the factor $\beta = \frac{v}{c}$. This distribution has its minimum for particles which have a $\beta\gamma \sim 3$ with $\gamma = \frac{1}{\sqrt{1-\beta^2}}$ irrespective of the particle as shown in Figure 3.7. Particle which have such an energy or slightly above it are called *Minimum-Ionizing-Particles* (MIPs).

The energy loss for a MIP in air is ~ 1.8 MeV per $\mathrm{g/cm}^2$, the number of particles N with energy E_0 is given by the integration:

$$N = \int_0^{E_0} \frac{\mathrm{d}E}{\mathrm{d}E/\mathrm{d}x}. \tag{3.4}$$

When considering the finite number of muons at a given energy and their lifetime of $\tau \sim 2.2\,\mu\mathrm{s}$, it could be expected that a muon travels a minimum of $\sim 600\,\mathrm{m}$ on average in vacuum. If time dilation is accounted for however, the muon's lifetime and thus it's travel distance are increased by a factor γ:

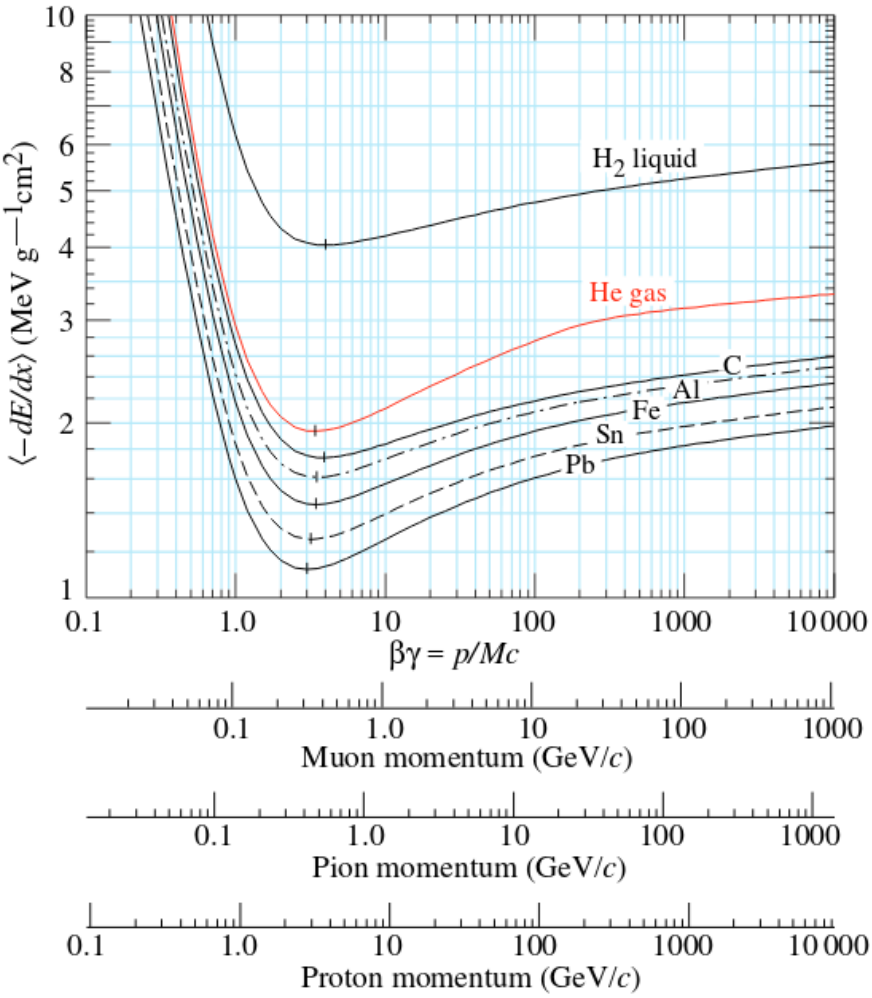

Figure 3.7: Mean energy loss rate in liquid (bubble chamber) hydrogen, gaseous helium, carbon,aluminum, iron, tin, and lead. Radiative effects, relevant for muons and pions, are not included.These become significant for muons in iron for $\beta\gamma \gtrsim 1000$, and at lower momenta for muons in higher-Z absorbers [8].

Altitude					Total intensity			Hard component			Soft Component		
Distance		Pressure			Omni-direct-ional	Verti-cal	Latitude effect	Omni-direct-ional	Verti-cal	Latitude effect	Omni-direct-ional	Verti-cal	Latitude effect
metres	feet	mm Hg	atm	m H_2O	particle /sea·cm^2	particle /sea·cm^2 ·sterad	%	particle /sea·cm^2	particle /sea·cm^2 ·sterad	%	particle /sea·cm^2	particle /sea·cm^2 ·sterad	%
0	0	760	1.000	10.33	0.020	0.015	10	0.013	0.000	10	0.007	0.000	10
2000	6561	59.6	0.781	8.11	0.033	0.025	16	0.018	0.012	15	0.017	0.013	15
4500	14764	43.3	0.870	5.59	0.10	0.07	25	0.08	0.020	25	0.07	0.06	25
10000	32808	10.8	0.201	2.60	0.7	0.3	45	0.10	0.05	30	0.6	0.25	30
16100	52822	7.60	0.100	1.04	1.5	0.5	75	0.23	0.08	?	1.25	0.42	80
30000	98425	0.87	0.0115	0.118	0.5	0.15	83	0.4	0.13	?	0.06	0.02	?
∞	∞	0	0	0	0.3	0.1	00	?	?	?	?	?	?

Table 3.1: Cosmic rays intensity at 50°.

$$\tau_{\mu\text{Lab}} = \gamma\tau_{\mu}. \tag{3.5}$$

As an example, muons with an energy of 3 GeV will have a $\gamma = \frac{E}{m} = \frac{3\,\text{GeV}}{105\,\text{MeV}} \sim 29$ leading to a lifetime $\tau \sim 62\,\mu$s. It would thus travel ~ 20 km in vacuum which corresponds to the approximate height of formation of muons in the atmosphere from pion decays. High-energy muons can make it to the earth's surface almost unhindered and easily pierce through 500 m of water.

This, in addition to magnetic deflection are the main reasons why the muon momentum-spectrum ($N(E) = \frac{K}{E^{\gamma}}$) at ground level is shifted towards high energies as shown in Figure 3.8.

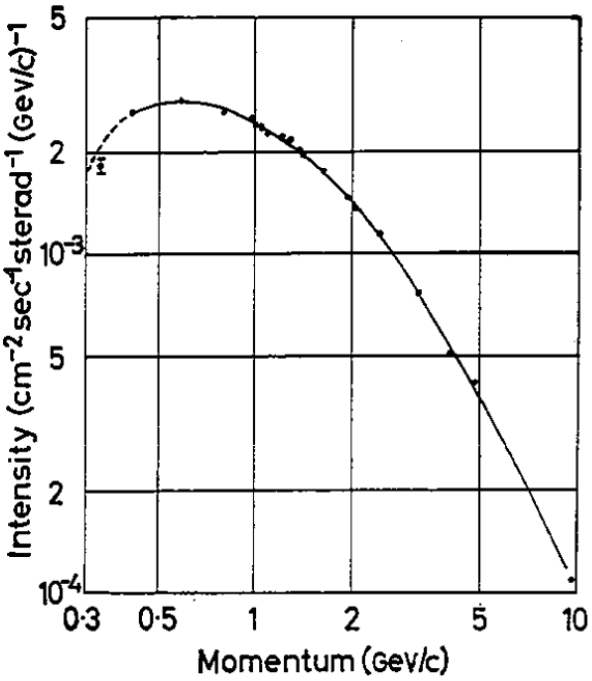

Figure 3.8: Vertical differential momentum of muons at 54° [2].

3.5 Cosmic ray intensity

In order to perform the experiment, it is necessary to know the width of each cosmic component, especially muons. Table 3.1 shows the muon flux as a function of relevant parameters. Figure 3.9 indicates the flux of various particle productions for different altitudes. At our latitude the muon asymmetry is about 1.3.

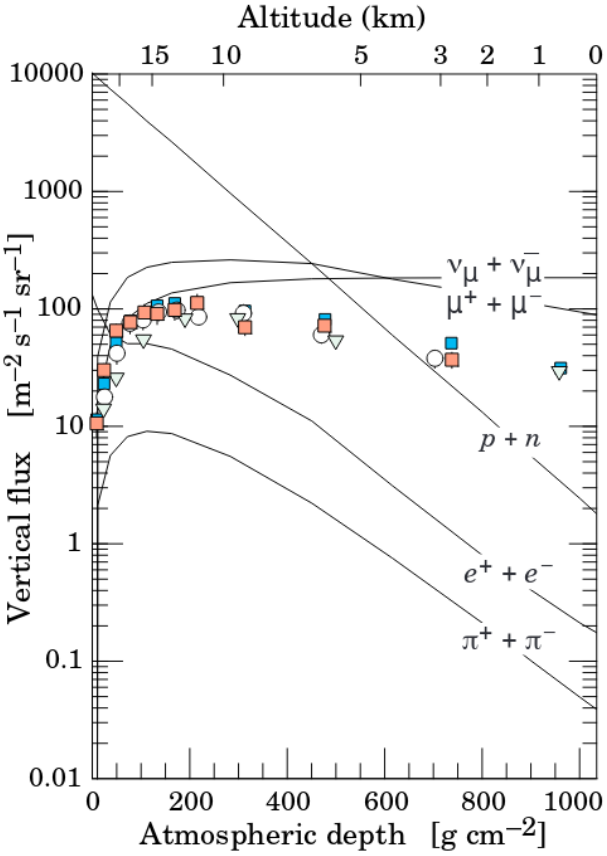

Figure 3.9: Vertical fluxes of cosmic rays in the atmosphere with $E > 1\,\mathrm{GeV}$ estimated from the nucleon flux. The points show measurements of negative muons with $E_\mu > 1\,\mathrm{GeV}$ [8].

Chapter 4

The muon

4.1 Muon history

Muons were discovered by Carl David Anderson and his student Seth Neddermeyer at Caltech in 1936 while they were working on cosmic rays. They observed that certain particles had a much more curved trajectory in their cloud chamber, than electron but less than protons. They were curving in the same direction as electrons meaning they had the same charge. They were initially mistaken for Yukawa's pion which supposedly mediated the strong interaction but were discovered not to have the right properties as it didn't interact strongly as it could traverse thick plates of metal unhindered. Heisenberg and Euler made the first computation of its lifetime in 1938, through the decreasing intensity as a function of travel distance. In 1947, Powell, Lattes, Muirhead and Ochialini used emulsion plates to discover two different "mesons": the π-meson and the μ-meson (which was later revealed to be quite different from its counterpart).

4.2 Muon production from pion decays

Pions are the lightest hadron and thus can only decay electroweakly, they are, as $q\bar{q}$ with antiparallel spins, spinless bound-states. Since they can only decay to fermions, which have spin $\frac{1}{2}$, only even-number-body-decays are allowed by angular momentum conservation laws. In addition, because of flavour conservation laws, leptons need to be produced as pairs or together with a(n) (anti)neutrino. An example pion decay is given in Figure 4.1.

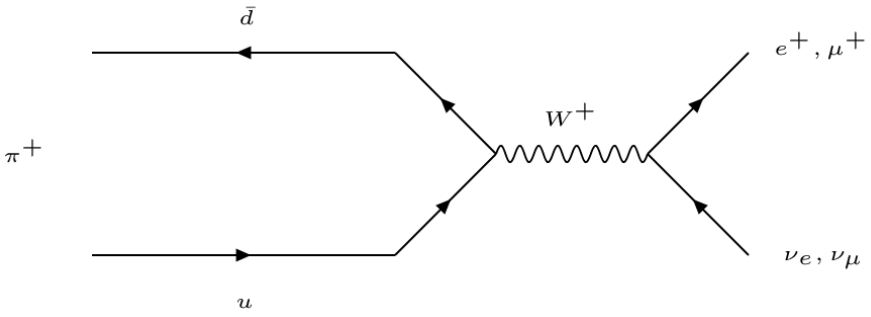

Figure 4.1: Positive pion decay.

There are thus 4 channels available for pions to decay:

$$\pi^+ \to \mathrm{e}^+ \nu_\mathrm{e}; \qquad \pi^- \to \mathrm{e}^- \overline{\nu}_\mathrm{e};$$

$$\pi^+ \to \mu^+ \nu_\mu; \qquad \pi^- \to \mu^- \overline{\nu}_\mu.$$

This gives rise to the branching ratio:

$$R = \frac{\text{Rate}(\pi \to \text{e}\nu)}{\text{Rate}(\pi \to \mu\nu)} = (1.230 \pm 0.004) \cdot 10^{-4}. \tag{4.1}$$

Muon-channel decays are thus nearly 10000 times more likely than electron-channel decays. This might be surprising when looking at energy phase space consirations: the muon being around 207 times heavier than the electron, the phase space would thus be:

$$R_{\text{phase-space}} = \frac{1 - \left(\frac{m_\text{e}}{m_\pi}\right)^2}{1 - \left(\frac{m_\mu}{m_\pi}\right)^2} \simeq 2.35. \tag{4.2}$$

with $m_\pi = 273 m_\text{e}$.

This wrong prediction is due to the lack of account taken from *V-A Coupling*, the combination of a vector (such as flight direction) and an axial vector (such as momentum) in the weak decay. This requires a new quantum number to be introduced: *Helicity H*, which is defined as the projection of spin on momentum:

$$H \doteq \vec{s} \cdot \hat{p} \qquad \text{with} \qquad \hat{p} = \frac{\vec{p}}{|\vec{p}|}.$$

Helicity expectation and alignement value are defined by:

$$\langle H \rangle \doteq \pm \frac{v}{c}.$$

With the expectation taking positive values for particles (e^-, μ^-,ν_e,ν_μ) and negatives ones for antiparticles (e^+,μ^+,$\overline{\nu}_\text{e}$,$\overline{\nu}_\mu$). It should be noted that in the Standard Model, only left-handed ($\langle H \rangle = -1$, spin and momentum antiparallel) neutrinos and thus only *right-handed* ($\langle H \rangle = +1$, spin and momentum parallel) antineutrinos exist. Neutrinos can be seen as practically massless and thus always travelling at the speed of light. This implies, through momentum and angular momentum conservation,that pions can only decay in certain configurations such as that shown in Figure 4.2.

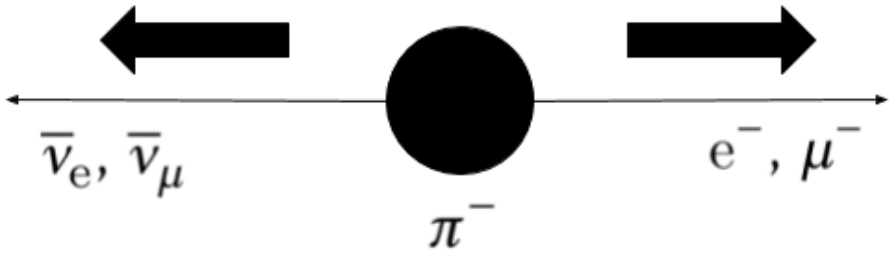

Figure 4.2: Spin and momentum in a negative pion's decay, as seen in the pion's rest frame.

Since the pion is spinless, the neutrino and charged fermion need to have opposite spin, since antineutrinos can only have right-handed helicity, the muon is emitted with right-handed helicity. However, only left-handed particles participate in the weak interaction. This can be seen in the right-handed helicity solution of the Dirac equation:

$$u_\uparrow = N \begin{pmatrix} \cos\frac{\theta}{2} \\ e^{i\phi} \sin\frac{\theta}{2} \\ \frac{|\vec{p}|}{E+m} \cos\frac{\theta}{2} \\ \frac{|\vec{p}|}{E+m} e^{i\phi} \sin\frac{\theta}{2} \end{pmatrix}. \tag{4.3}$$

The left-handed chirality projector is given by:

$$P_{\mathrm{L}} = \frac{1}{2}(1-\gamma^5) = \frac{1}{2}\begin{bmatrix} 1 & 0 & -1 & 0 \\ 0 & 1 & 0 & -1 \\ -1 & 0 & 1 & 0 \\ 0 & -1 & 0 & 1 \end{bmatrix}. \tag{4.4}$$

with, when applied to the spinor yields:

$$P_{\mathrm{L}} u_{\uparrow} = \frac{N}{2}\Big(1 - \frac{|\vec{p}|}{E+m}\Big) u_{\mathrm{L}}. \tag{4.5}$$

which tends to zero in the limit $m << E$, while

$$P_{\mathrm{R}} u_{\uparrow} = \frac{N}{2}\Big(1 + \frac{|\vec{p}|}{E+m}\Big) u_{\mathrm{R}}. \tag{4.6}$$

tends to u_{R} in the limit $m << E$. This leads to

$$u_{\uparrow} = P_{\mathrm{R}} u_{\uparrow} + P_{\mathrm{L}} u_{\uparrow} = \frac{1}{2}\Big(1 + \frac{|\vec{p}|}{E+m}\Big) u_{\mathrm{R}} + \frac{1}{2}\Big(1 - \frac{|\vec{p}|}{E+m}\Big) u_{\mathrm{L}}. \tag{4.7}$$

in the limit $E >> m$, the right-handed chiral and helicity states are identical as expected. Even though only left-handed chiral particles participate in the weak interaction, the right-handed contribution isn't necessarily zero. The matrix element is expected to be proportional to the left-handed chiral component of the right-handed helicity fermion spinor:

$$\mathrm{M}_{fi} \propto \frac{1}{2}\Big(1 - \frac{|\vec{p}|}{E+m}\Big) = \frac{m}{m_\pi + m}. \tag{4.8}$$

The calculation of the branching ratio

$$R = \frac{P(\pi \to \mathrm{e}\nu)}{P(\pi \to \mu\nu)} \simeq \frac{m_{\mathrm{e}}^2}{m_\mu^2} \frac{(1 - \frac{m_{\mathrm{e}}^2}{m_\pi^2})^2}{(1 - \frac{m_\mu^2}{m_\pi^2})^2} \simeq 1.283 \cdot 10^{-4}. \tag{4.9}$$

Which is in good agreement with experimental observations. For this measurement, it is necessary that muon in the pion rest-frame be entirely left-handed. The Lorentz transform into the Lab-frame allows for this in this experiment.

4.3 Muon polarization in cosmic rays

In this experiment, muons will be stopped in a 25 mm thick copper plate. If other present materials are accounted for, such as the lead shielding, concrete ceilling and 20 km, only "slow" muons, with an energy estimated to be of ~ 609 MeV are actually stopped in the copper. While this might be an estimate, Figure 4.3 demonstrates the relative constance of polarization at energies between 300 MeV and 900 MeV.

Muons of such energies can be created in two different ways (in the following, positive muons will be looked at):

- They can be produced in 616 MeV pions and are then emitted in the direction of flight, with negative helicity and upward-facing spin (Figure 4.5a).
- They can be produced in 1058 MeV pions and are then emitted against the direction of flight, with positive helicity and downward-facing spin (Figure 4.5b).

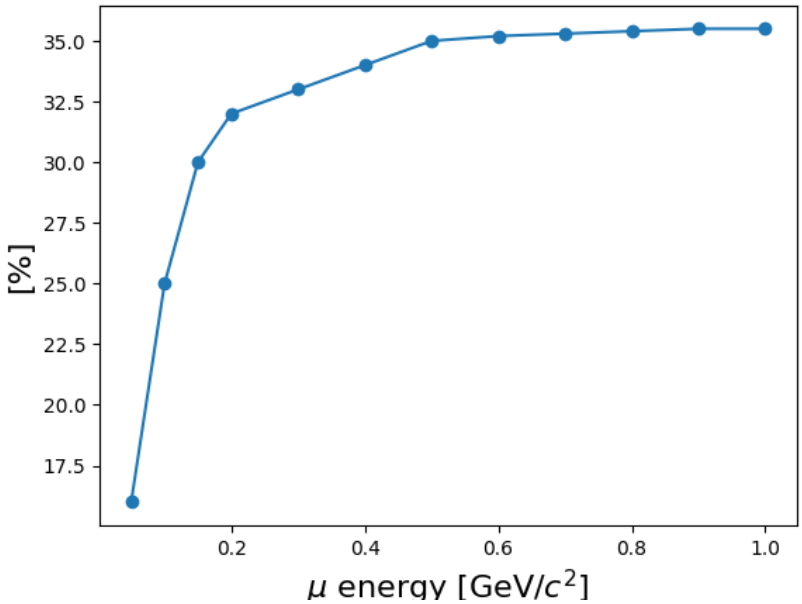

Figure 4.3: Muon polarization as a function on energy.

Figure 4.4: Muon polarization as a function on energy.

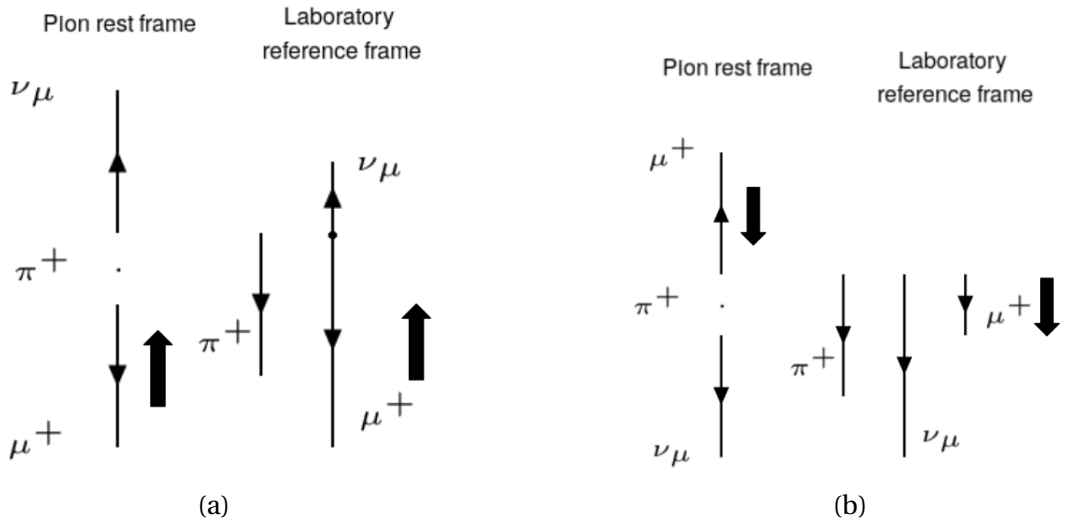

(a) (b)

Figure 4.5: Production of 609 MeV in cosmic radiation with (a) negative helicity and (b) positive helicity.

With a uniform pion energy distribution, it was first impossible to observe polarized muons. At the aforementionned energy ranges however, the pion abundance as a function of energy $N(E)$ can be seen to display the following behaviour:

$$N(E)\mathrm{d}E \sim E^{-1.4}\mathrm{d}E. \tag{4.10}$$

Thus the ratio of muons with positive helicity $N(\downarrow\uparrow)$ to those with negative helicity $N(\uparrow\uparrow)$ is:

$$\frac{N(\downarrow\uparrow)}{N(\uparrow\uparrow)} = \frac{616^{-1.4}}{1058^{-1.4}} \simeq \frac{2.15}{1}. \tag{4.11}$$

An excess of muons with negative helicity is thus of polarization is expected. The polarization P is defined as:

$$P \doteq \frac{N(\downarrow\uparrow) - N(\uparrow\uparrow)}{N(\downarrow\uparrow) + N(\uparrow\uparrow)}. \tag{4.12}$$

It is thus expected to find a muon polarization of about 37%.

4.4 Muon decays

Muons decay with an average lifetime of $2.2 \cdot 10^{-6}$s into the lighter flavoured lepton, the electron. Since muons are stopped in copper and that the process is different for positive and negative muons, both processes will be treated separately.

4.4.1 The decay of free μ^+

Positive muons remain in the free interstices and can thus decay like free muons. In order to preserve lepton number, the following decay takes place:

$$\mu^+ \rightarrow \mathrm{e}^+ + \nu_\mathrm{e} + \overline{\nu}_\mu.$$

As a three-body decay, the positron's momentum spectrum is continious, however, due to the parity-violating nature of the weak interaction, an asymmetry in the positron's angular distribution can be found as shown in Figure 4.6

For the transition probability W for the solid angle Ω:

$$\mathrm{d}W = \frac{G_\mathrm{F}^2 m_\mu^5 c^4}{192\pi^3\hbar^7}\left[2\epsilon^2(3-2\epsilon)\right]\left[1+\frac{1-2\epsilon}{3-2\epsilon}\cos\Theta\right]\left[\frac{1-n_\mathrm{e}s_\mathrm{e}}{2}\right]\mathrm{d}\epsilon\frac{\mathrm{d}\Omega}{4\pi}, \tag{4.13}$$

with $\epsilon = \frac{E_\mathrm{e}}{E_\mathrm{max}}$, $E_\mathrm{max} = \frac{1}{2m_\mu c^2}$ and Θ the angle between the muon's spin and the positron's momentum. The first block between brackets provides the positron momentum spectrum, the second provides the angular distribution and the third represents the positron helicity in the V-A description. The third block can be approximated with $\frac{v_\mathrm{pos}}{c} \sim 1$ and thus can be neglected. For the number of positron emitted at an angle Θ one can write:

$$N(\Theta) \sim 1 + a\cos\Theta \text{ with the assymmetry factor } a = \frac{1-2\epsilon}{3-2\epsilon}. \tag{4.14}$$

The average assymmetry over all energies can be integrated from Equation 4.13:

$$N(\epsilon) \sim \int_0^1 \left[2\epsilon^2(3-2\epsilon)\right]\left[1+\frac{1-2\epsilon}{3-2\epsilon}\cos\Theta\right]\mathrm{d}\epsilon \implies N(\Theta) \sim 1 + \frac{1}{3}\cos\Theta. \tag{4.15}$$

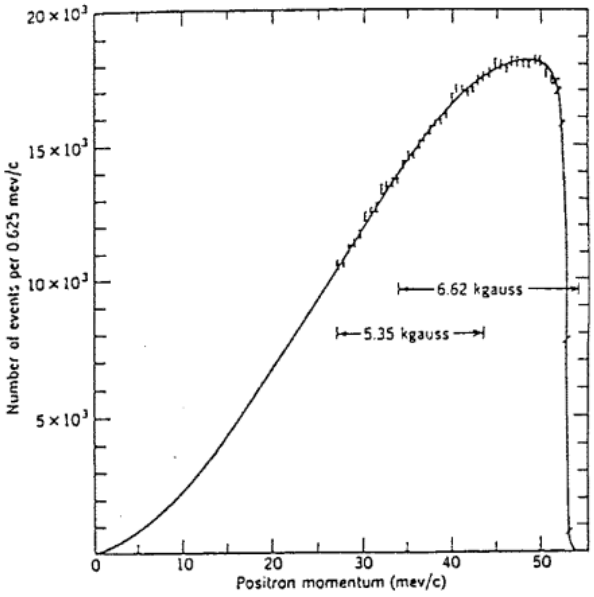

Figure 4.6: Final state positron from muon decays momentum spectrum.

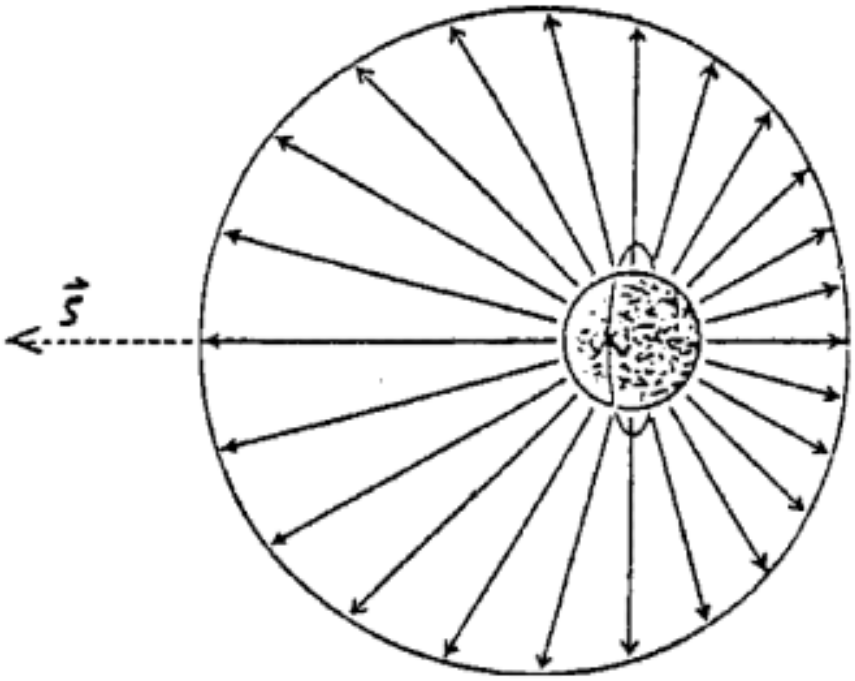

Figure 4.7: Illustration of positron angle emission in muon decays. The length of the arrow is proportional to the emission probability for that angle.

This corresponds to an assymmetry of ~ 33%. This is illustrated in Figure 4.7.

In order for them to be detected, the positrons first need to exit the copper plate which, depending on their emission angle and the decay vertex position, requires a minimal energy of 30 MeV. This leads to an assymmetry factor $a = 0.38 \pm 0.04$ [3]. The oberserved assymmetry in this measurement also depends on the Polarization P of the muon:

$$N(\Theta) \sim 1 + aP\cos\Theta. \tag{4.16}$$

The last remaining unknown if the muon's lifetime τ_μ. Integrating Equation 4.13 over space and energy provides the transition probability W which is nothing else than the *inverse lifetime*:

$$W = \frac{G_F^2 2 m_\mu^5 c^4}{192\pi^3\hbar^7} = \frac{1}{\tau_\mu}. \tag{4.17}$$

Litterature places this lifetime at $2.197 \cdot 10^{-6}$s. By measuring the muon's lifetime, one can thus also obtain a value of Fermi's coupling constant G_F.

4.5 Nuclear capture of negative muons

As opposed to antimuons, muons are mostly captured by nuclei. This process takes place after the muons are decelerated through ionization processes from the speed of light to approximately $6 \cdot 10^{-3} c$ ($\simeq 2$ keV) in $\sim 10^{-9}$ s. They are then captured by the atom in around 10^{-13} s. The muon then cascades through the K-Shell in a time proportionnal to Z^4 with Z the number of protons in the nucleus. This time ranges from 10^{-9} s for Uranium to 10^{-17} s for Hydrogen. As the muon and electrons are otherwise identical particles, the orbit radius of muon-shells is calculated in the same way as that of electrons except for one thing: due to the 207 mass-factor difference between electrons and muons, the muon's Bohr radius is 207 times smaller which implies a much more overlapping between the nucleus' and muon's wavefunctions. This implies a high probability of nuclear capture through the process:

$$\mu^- + \mathrm{p} \rightarrow \mathrm{n} + \nu_\mu. \tag{4.18}$$

Thus the total decay probability W is calculated from the sum of the initial probability W_i and the decay probability W_d in the K-Shell: $W = W_\mathrm{i} + W_\mathrm{d}$. As such, the lifetime of negative muons τ_- is calculated as:

$$\frac{1}{\tau_-} = \frac{1}{\tau_\mathrm{d}} + \frac{1}{\tau_\mathrm{i}}, \tag{4.19}$$

with $\tau_\mathrm{d} = \frac{1}{W_\mathrm{d}}$ and $\tau_\mathrm{i} = \frac{1}{W_\mathrm{i}}$. The probability W_i scales as:

$$W_\mathrm{i} = W_\mathrm{d}\left(\frac{z_\mathrm{eff}}{z_0}\right)^4, \text{ with } z_0 = 10.8. \tag{4.20}$$

z_eff is here the effective nuclear charge which for copper ($Z = 29$) is:

$$z_\mathrm{eff} = z(1 + (\frac{z}{42})^{1.47})^{\frac{-1}{1.47}} \simeq 21. \tag{4.21}$$

Assuming that the decay probability of the negative muon in a K-Shell is identical to that of a free muon ($\frac{1}{\tau_+}$), then according to Equations 4.19 and 4.20, the average lifetime τ_- of negative muons:

$$\tau_- = \tau_+ \frac{z_0^4}{z_0^4 + z_\mathrm{eff}^4}. \tag{4.22}$$

For copper this is roughly $\tau_- = 144\,\text{ns}$. For nuclei with low charges, the difference in the average lifetimes is small (for Carbon, $\tau_- = (0.1635 \pm 0.0024)\,\mu\text{s}$). μ^- is in this measurement measured indirectly through the detection of the β from excited Nickel nuclei which arise from copper nuclei:

$$\begin{aligned} \mathrm{p} + \mu^- &\rightarrow \mathrm{n} + \nu_\mu \\ (\mathrm{Cu} + \mu^- &\rightarrow \mathrm{Ni}^* + \nu_\mu) \\ &\hookrightarrow \mathrm{Ni}^* \rightarrow \mathrm{Cu} + \mathrm{e}^- + \overline{\nu}_\mathrm{e} \\ &(n \rightarrow \mathrm{p} + \mathrm{e}^- + \overline{\nu}_\mathrm{e}) \end{aligned} \tag{4.23}$$

Since this process is quite fast, the electron is seen at about the same time as the muon.

4.6 Muon magnetic moment

The muon, as a fermion (particle with $s = \frac{1}{2}$) and charge e has a magnetic moment:

$$\mu_\mu = \frac{e\hbar}{2m_\mu}, \text{ in litterature, } \mu_\mu = 4.49045 \times 10^{-26}\,\mathrm{J\,T^{-1}}. \tag{4.24}$$

In a B-field with flux-density B, the muon spin precesses with a *Larmor-Frequency* ω_L:

$$\omega_\mathrm{L} = g\frac{eB}{2m_\mu} = g\frac{\mu_\mu B}{\hbar}. \tag{4.25}$$

For our purpose, the muon's $g - Factor$ can be approximated to $g = 2$ ($g - 2 = 11659208.9 \pm_{\text{stat}} 5.4 \pm_{\text{syst}} 3.3 \cdot 10^{-10}$ [8]). The Larmor Frequency is then approximately $85.14\,\mathrm{kHz\,G^{-1}}$. In particular, because of their spin, emitted positrons precesses in the same direction as their emission direction.

Chapter 5

Experimental apparatus

The working principle of this experiment is based on one of Rasetti's 1941 experiments where he first measured resting muon's lifetime through a coincidence circuit.

5.1 Experimental principle

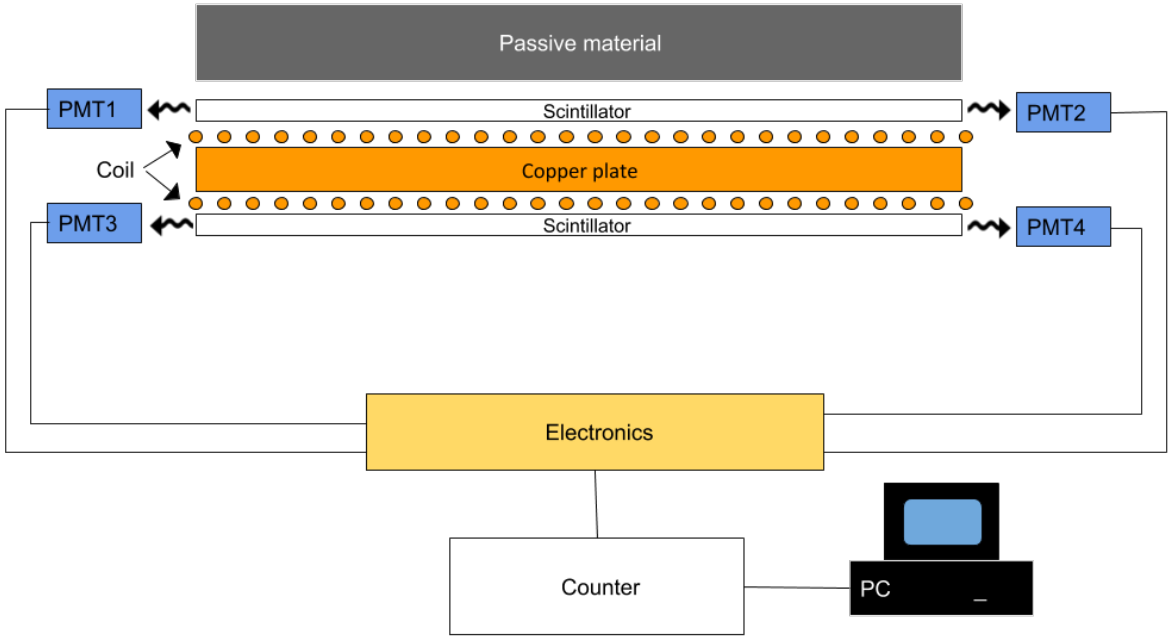

Figure 5.1: Illustration of the experimental apparatus.

The experiment's principle is described in Figure 5.1. The Copper target stops muons and is placed inside a magnetic field. The muon's lifetime is measured by looking at the time between a muon's stopping and the emission of a positron. The preferred direction and the Larmor frequency must also be registered in order to determine the magnetic moment. Particles are detected through scintillator plates. Scintillators are materials which, when ionized, will rearrange their electronic structures and emit photons at set energies. Those scintillators are isiolated from external luminous interference, connected to wave guides and then further to photomultipliers (here

Photo-Multiplier-Tubes or PMTs), which then convert the light signal into an electronic one. The time differences are then saved on a PC. In other to provide further shielding to the experiment, a 5 cm layer of dense and passive material (here lead) is added on top of the experiment.

A muon stop is experimentally defined as an electronic signal from the coincidence circuit of $PMT1$ and $PMT2$ but none from that of $PMT3$ and $PMT4$. Indeed an unstopped muon would traverse both scintillator layers and would thus register a signal in both coincidence circuits while a stopped one would traverse the top layer and not the bottom one. In logic language, a stopped muon would thus be written as:

$$(PMT1 \textbf{ AND } PMT2) \textbf{ AND } (\overline{PMT3 \textbf{ AND } PMT4}). \tag{5.1}$$

Two PMTs and a coincidence circuit are used so as to rule out random events and reduce electronic background. Muons generate strong photon bursts that can be seen by both PMTs. A muon decay is defined in the same way as a muon stop meaning that when a particle is sent downwards, it isn't registered, leading to a loss in statistics.

Nevertheless, this logic circuit is used because there would otherwise be no spatial resolution and thus no way to determine the muon spin which is needed for the magnetic moment determination. Since muon stops and decays are registered as the same signal, the two events need to be separated through their sequence:

- A muon decay is a stochastic process which thus is distributed according to an exponential probability distribution. For an average lifetime of $\tau = 2.2\,\mu s$ we get a half-life $\lambda = \frac{\tau}{\ln(2)} \simeq 1.5\,\mu s$, therefore 99% of muons decay after $10\,\mu s$.
- Due to the low vertical radiation intensity, the average distance between two muons is $\sim 10\,s$ which is about 10 times the $12.5\,\mu s$ readout length. This reduces the likelihood of two overlapping events.

Thus, an event is identified as a muon-stop if and only if a second event takes place in the next $12.5\,\mu s$ which then defines a decay. All other events are discarded.

5.2 Target and B-field

Muon are captured in a 1 m long, 50 cm wide and 2.5 cm thick copper plate. Copper as a material has the following advantages justifying its use:

- It is slightly diamagnetic ($\chi_m = -7.4 \cdot 10^{-6}$) and thus has little influence over the magnetic field.
- Its thickness allows it to effectively stop muons.
- The muons are not depolarized by the formation of muonium.

The coil used in this experiment is 1 m and composed of 456 loops. The calibration curve in Figure 5.2 shows the need for 10 A for 48 G (calibration $B[Gauss] = 4.72\,I$) and thus, a 4.1 MHz Larmor Frequency ω_L. This corresponds to a period $T = \frac{2\pi}{\omega}$ so $\sin 1.5\,\mu s$, which, with a time resolution of $0.05\,\mu s$ and a window of $12.5\,\mu s$, such as in this experiment, theoretically 7-8 periods should be observed.

The magnetic field must however be homogenous enough that two muons stopped at different locations don't have too big of a phase difference. If the relative phase difference should be $\Delta\omega T \leq 0.3$, with T being the measurement period (i.e. $12.5\,\mu s$). In this case, equation 4.25 implies that the homogeneity of the B-field at 48 G must satisfy $\frac{\Delta B}{B} \leq 0.008$. If one uses the law of Biot-Savart

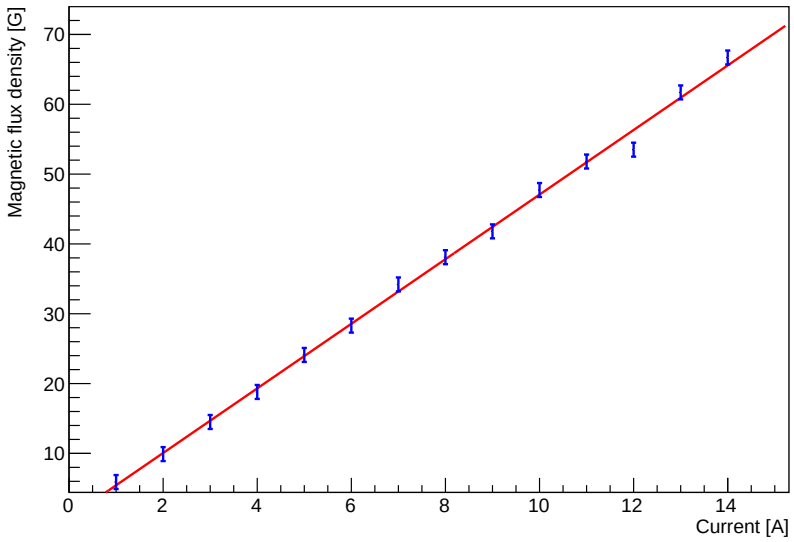

Figure 5.2: Calibration curve of the magnetic field as measured with a fluxgate compass.

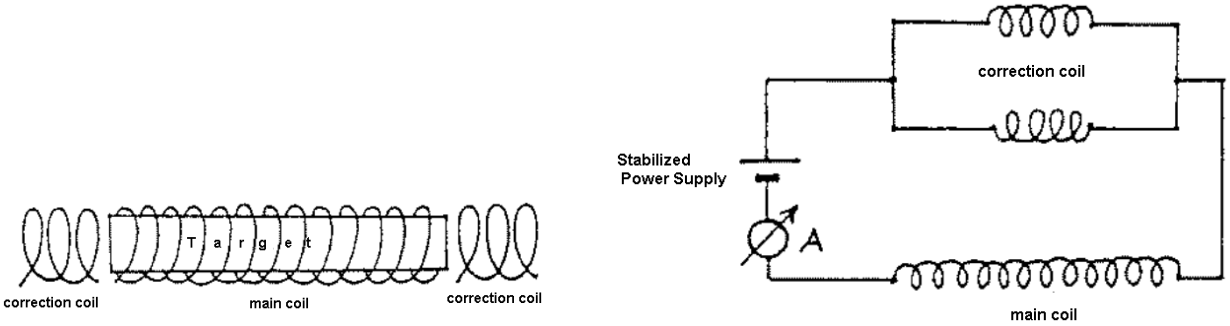

(a) (b)

Figure 5.3: (a) Magnetic coil structure. (b) Magnetic coil circuit.

to compute the magnetic field, they would find $\frac{\Delta B}{B} = 0.013$. An additional 10 cm long correction coil at each end of the main coil improves the value to 0.008. Calculations with different current values show that this value represents an absolute minimum for this arrangement and is achieved precisely when the correction coil current is half of that of the main coil. The secondary coils are thus connected in parralel to each other and in series with the main one as shown in Figure 5.3.

The homogenity of the magnetic field is shown in Figures 5.4 5.5. The temporal stability of the magnetic field's current is ensured through a stabilized power supply up to 0.5%. The deterioration of $\frac{\Delta B}{B}$ by a further 0.005 such as to not observe the muon's polarization over the measurement period of 12.5 µs. In order to cool the coil, which is always powered at 10 A, a ventilator, which **always needs to be turned on when the B-field is in use**, is used.

5.3 Particle detection apparatus

The scintillators above and below the copper target are of type NE110 (organic scintillator) have a surface of $90 \times 45\,\text{cm}^2$. As the ionizing particles pass through the scintillator, the molecular electron states are being excited, this leads to de-excitation with emission of UV light. Since the absorption length of this UV light is very short, it will be absorbed by another scintillator atom which will lead to a similar electronic process and the isotropic emission of another, shorter wavelength flu-

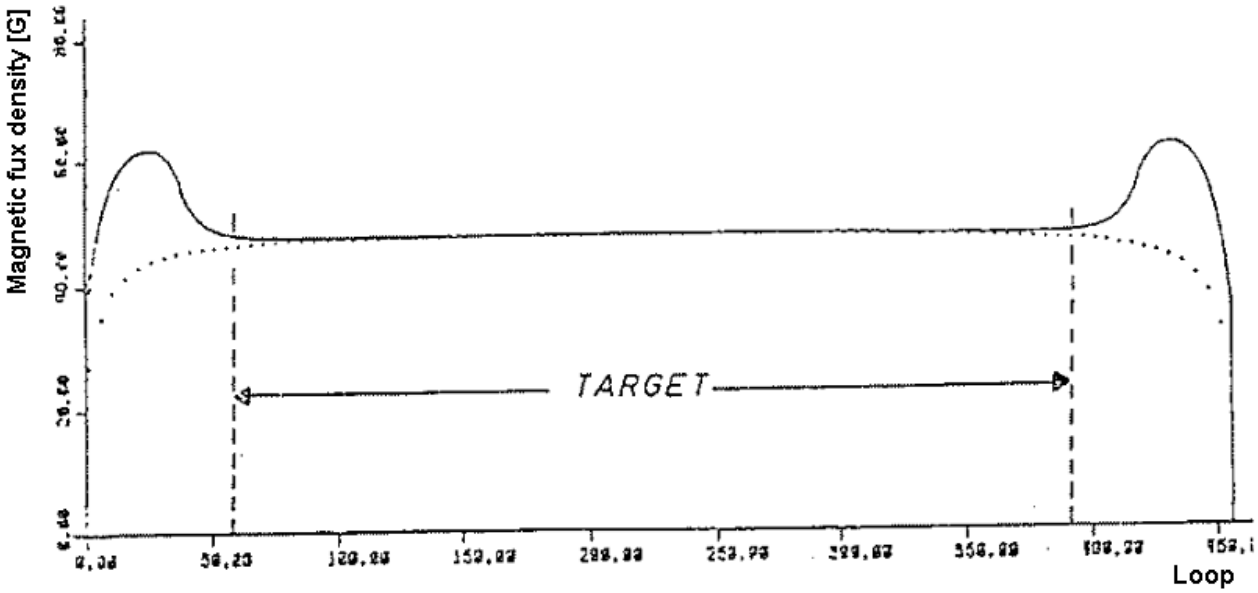

Figure 5.4: Magnetic field as calculated along the coil at 10 A.

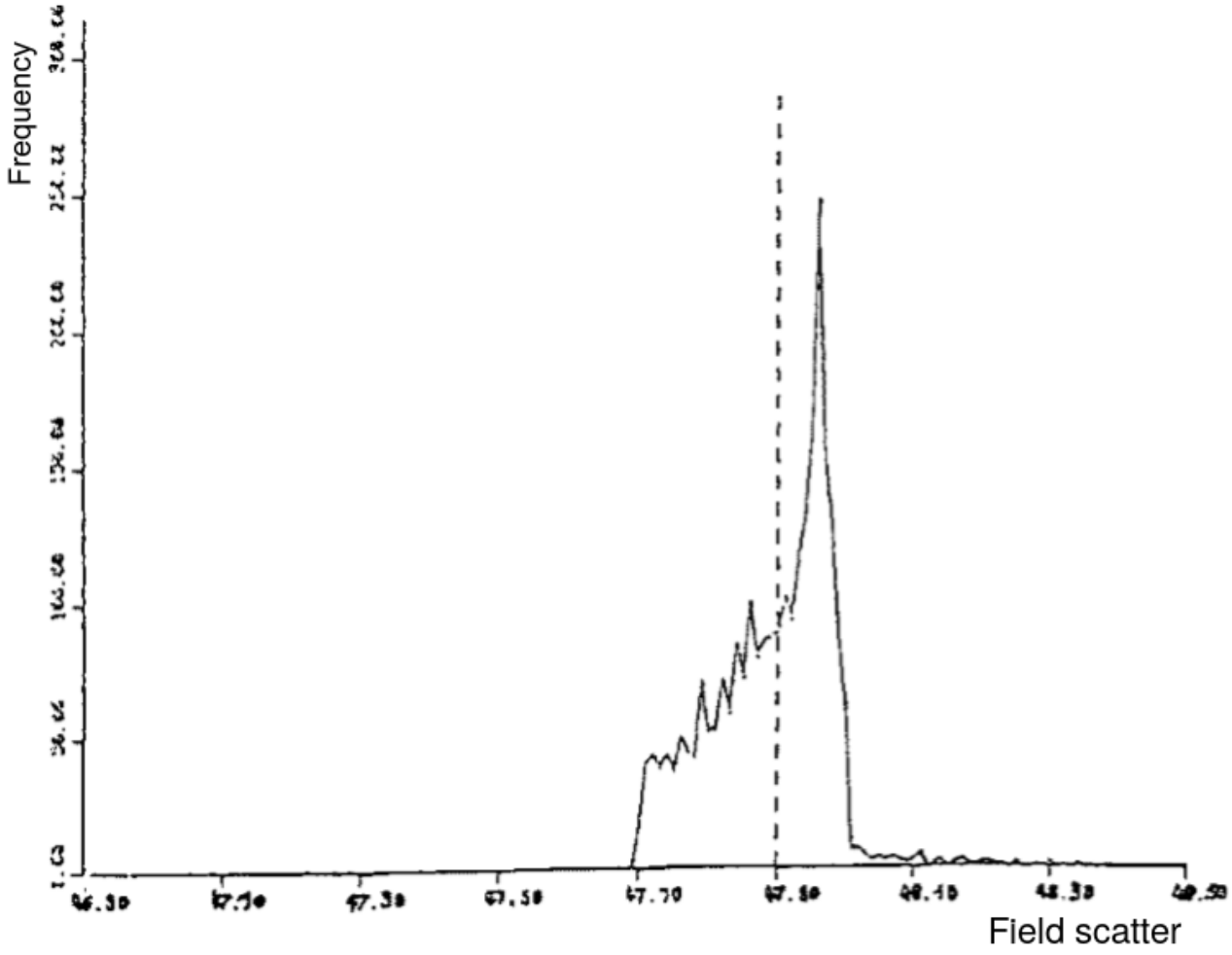

Figure 5.5: Scatter of the B-field as calculated along the coil axis for a 10 A current. The dotted line represents the average scatter.

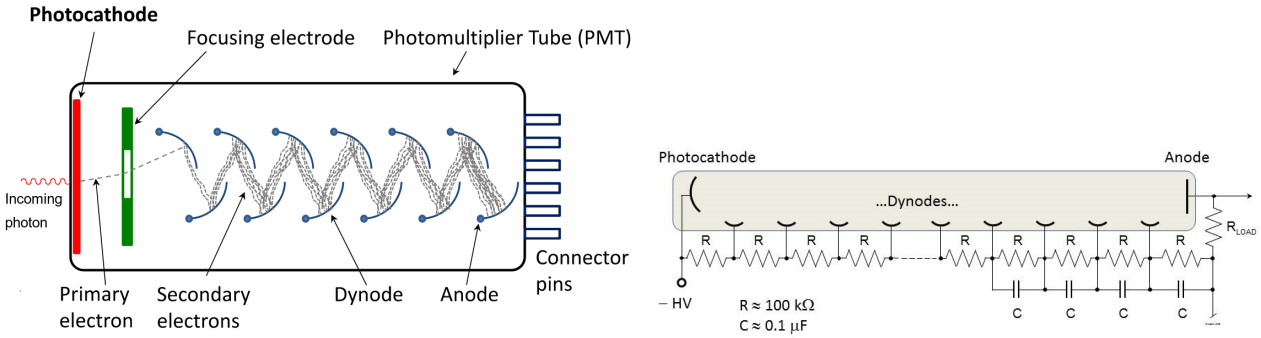

(a) (b)

Figure 5.6: (a) PMT schematic illustration. (b) PMT example voltage divider circuit [6].

orencence photon. It is thus also called a wavelength shifter. The fluorescent decay time is of the order of 10^{-10} s. In order to reduce loss of signal, the scintillator surface is polished and covered in aluminized foil, allowing photon reflexion and limitingphoton escape. In other to deal with background from ambient light, photographic paper covered in black foil forms an outer layer of the scintillator units.

5.4 The photomultiplier

The light produced in the scintillators is guided in a plexiglas waveguide to a photomultiplier. A photomultiplier is an electronic detector used to convert light into electrons. The photomultipliers used here are Photo-Multiplier-Tubes (PMT) shown in Figure 5.6, a widely used technology for light detection. The photomultiplier tube is based on a thin vapor-deposited conducting layer photocathode which converts photons to electrons via the photoelectric effect, these electrons are then passed through a focusing electrode directing them towards a dynode circuit serving to amplify the electron signal via secondary emission [1]. Each dynode is held at at slightly higher (~ 100 V) potential than the preceding one. When an electron strikes a dynode, it will cause emission of low energy electrons which will then be accelerated towards the next dynode. The geometry of the dynode circuit is such that a cascade occurs with an exponentially increasing number of electrons being produced at each dynode. The final dynode is connected to an anode. At this stage, a large number of electrons reach the anode, it will thus create a sharp rising edge which is an easy analog signal to detect. The voltage distribution in the dynodes is done through a voltage divider circuit. The photocathode is generally held at a negative high voltage of order 1000 V, while the anode is very close to ground potential. The capacitors across the final few dynodes act as local reservoirs of charge to help maintain the voltage on the dynodes while electron avalanches propagate through the tube. It should be noted that the design shown in Figure 5.6b is only an example as many different such circuits exist.

5.5 Electronics

5.5.1 Introduction to signal electronics

Electronics have historically worked around analog signals. These signal are the products of direct physical effects (typically electron/ion drift reaching the anode/cathode and creating a current). An analog signal is thus a continuous (sinusoidal) wave which is changing over a time period. They are typically described by their amplitude, period (or equivalently frequency) and phase, they have no fixed range and as a result are more unstable. A good example of an analog signal is the

human voice which can modulate it's amplitude (volume), frequency (pitch) and phase (spacing) to transmit information.

With the introduction of vacuum tubes and logic circuits, it became possible to produce and process binary signals. These function around sharp rising and falling edge signals, so-called gate functions which (in an ideal scenario) instantly pass from a reference, fixed, low voltage level (usually 0 V) to a reference, fixed, high voltage. The corresponding electronics is then able to reckognize the change of voltage and act accordingly through boolean algebra of varying complexity. Digital signals are represented through bit rates and bit intervals, have a very well-defined and limited range (such as 0 and 1). They are as a result less prone to distortion and interference. Computers are among the best examples of digital signal carriers.

5.5.2 Experiment logic

The PMTs emit short, fast, subsequent (analog) electronic impulses, the electronics are used to discriminate muon-stop signals. This happens with a coincidence circuit. A coincidence can be seen as a an "electronic binary operator" (through an **AND** gate, thus), it thus takes two signals as inputs which in the case of the Nuclear Instruments Module (NIM), take gate signals with binary values of 700 mV (logical 1/**TRUE**) or 0 V (logical 0/**FALSE**). It provides a fixed output based on the mode of operation either a gate signal or a logical 0. The coincidence can be operated as **AND** ($\odot$), **OR** ($\oplus$), **NAND** (=$\overline{\textbf{AND}}$) or **NOR** (= $\overline{\textbf{OR}}$). The output signal depends on the input algebra logic which can be found in Table 5.1.

The conditions for a muon stop or decay from Figure 5.1 can be written:

$$\big(\text{PMT1} \odot \text{PMT2}\big) \odot \big(\overline{\text{PMT1}} \oplus \overline{\text{PMT2}}\big). \tag{5.2}$$

The first block represents a logical **AND** while the second one represents a logical **NOR** (see Table 5.1). The entire logical circuit, including the **AND** is realized in the electronic circuit shown in Figure 5.7 in coincidences 1,2 and 3. The logical units used to make coincidences require sharp rectangular gate (digital) pulses which is why the analog PMT signal is connected to discriminators after amplification.

Similarly to coincidences, discriminator output lengths can be varied. Discriminators also include the possibility to separate interference pulses (noise) from signal: they will only deliver a gate signal if the signal input exceeds a certain threshold which can be set. The rest of the circuit after coincidence 3 is used to set a counter to measure the decay time, from the start of a muon-stop (Reset) and stop at the subsequent event (interrupt) if this occurs within the fixed 12.5 µs. The counter reset and the 12.5 µs wide time window are implemented via the monoflop. A monoflop has one input (s) for start (as the reset is only used when operating as a flip-flop) and three outputs:

- o (out) produces a gate output of variable length caused by an input and a 0 V output otherwise.
- $\overline{o}$ ($\overline{\text{out}}$) which produces an opposite signal to o.
- e (end) sends a short gate output of fixed length (per example 10 ns) when the output signal has ended.

The monoflop open with a 12.5 µs gate for coincidence 5 and blocks coincidence 4 so that the reset switch isn't hit during the measurement period. Coincidence 5 is then ready for 12.5 µs to receive the second, supposedly delayed second signal from coincidence 3 and thus stop the counter.

The variable delay between monoflop and coincidence is achieved through an extra cable. It is crucial that signals from coincidence 3 nd the monoflop be perfectly spaced out since the start

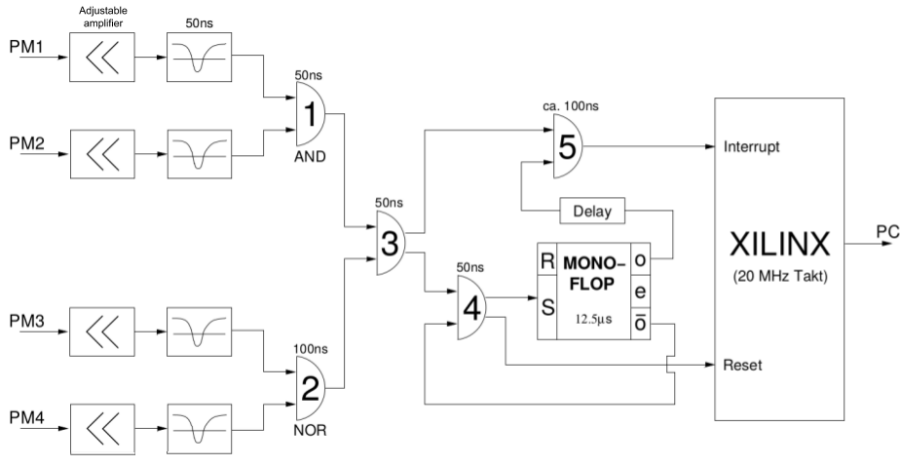

Figure 5.7: Electronic circuit of the experiment.

Input S_1	Input S_2	**AND** ($\odot$) output	**OR** ($\oplus$) output	**NAND** ($\overline{\textbf{AND}}$) output	**NOR** ($\overline{\textbf{OR}}$)
1	1	1	1	0	0
1	0	0	1	1	0
0	1	0	1	1	0
0	0	0	0	1	1

Table 5.1: Coincidence logic table.

signal cannot be allowed to overlap with the gate so as to immediately trigger a reset. On the other hand, dead time between the start signal and the start of the gate (which is accepted as a stop) cannot take place either.

5.6 Time measurement

The time between the first, muon-stop, signal and the ensuing signal (muon decay) will be determined with a *Time to Digital Converter* (TDC). This TDC is done with a *Field Programmable Gate Array* (FPGA) from XILINX. An FPGA can be seen as an array of programmable logic blocks not unlike the coincidences described earlier. The blocks and their connections are programmed in by the user. Interactions with the outside world is done through I/O blocks. A network of programmable connections is available for connections between individual blocks.

The TDC is here programmed so as to function similarly to an 8-bit counter, which is reset through the aforementionned Reset-signal. Until the interrupt signal is received, the value of the counter is incremented by one unit for every XILINX board cycle. The clock frequency of the board is 20 MHz which corresponds to a counting unit of 50 ns and thus yields a maximum counted time difference is 12.8 µs. If the interrupt signal is received within this time, the counter's value is readout by the software on the connected PC and converted into a time value.

5.7 Data acquisition with the PC

4-5 events/min are expected. This counting rate thus requires to extend the measurement period to a week in order for enough statistics to be gathered. The DAQ program works as follows: when the XILINX obtains a valid event, its counter's value is sent to the PC and converted there into a time value. This value is then histogrammed which has 256 bins of 50 ns, corresponding to the range of all possible values that can be outputed by the TDC. The time measurements are then

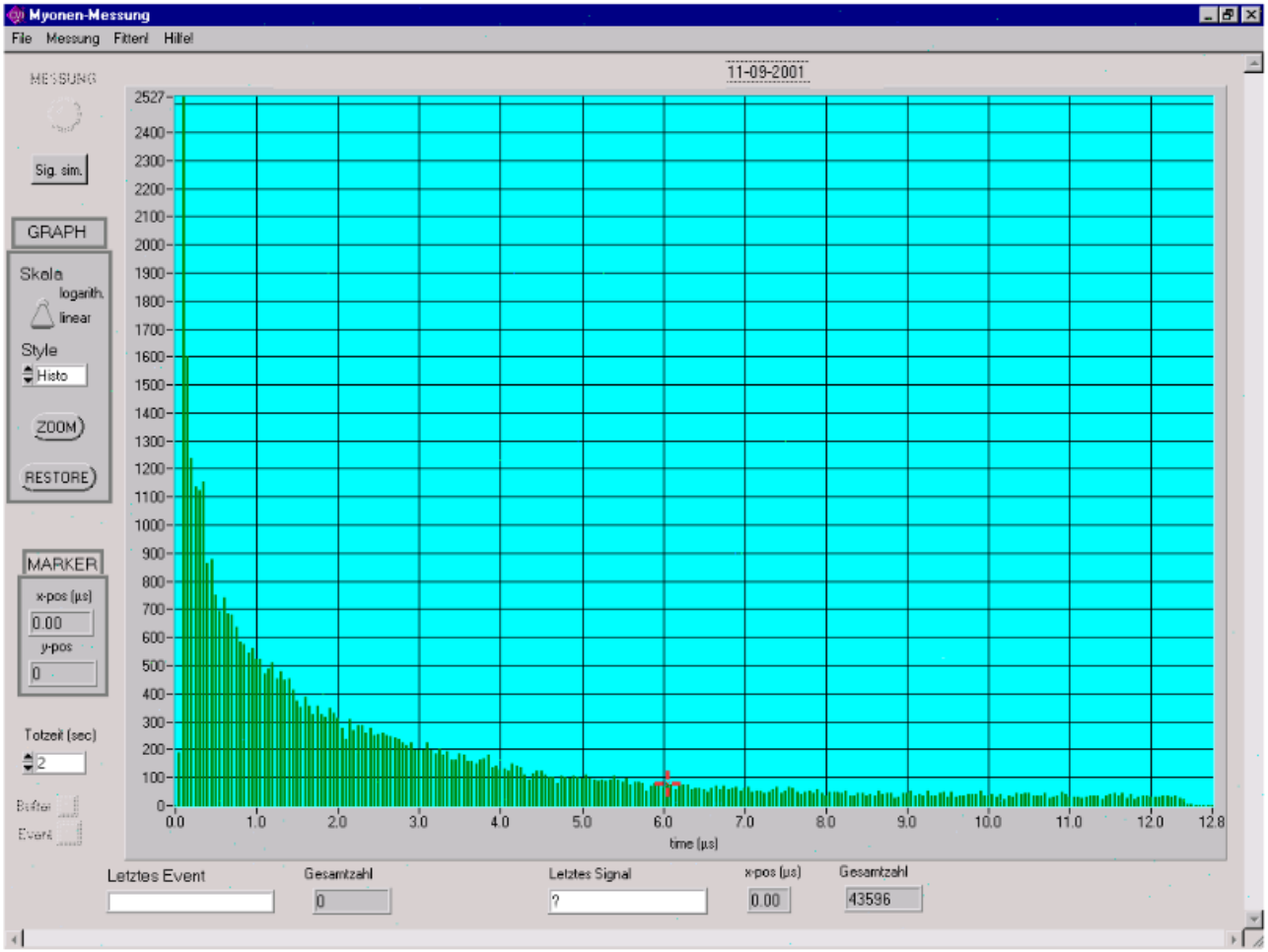

Figure 5.8: Measurement software window.

plotted and saved for every event (allowing for data recovery in the case of a crash or the like). The data is written into files which can be then easily be read-out. The DAQ software is in german but a measurement can be started by going into *Messung→Beginnen* and ended through *File→Beenden*, the measurement GUI and window can be found in Figure 5.8.

Chapter 6

Measurement and analysis

6.1 Preparatory measurements

Before the actual measurement can be understaken, a couple of preparations must be made such as setting the PMT voltages, the discriminator thresholds and finally testing the electronics with simulated pulses.

6.1.1 Setting the counter

The discriminator's rectangular pulse widths are set to 50 ns, this provides long enough pulses for the coincidences while also minimizing the amount of random coincidences which arise from the overlap of two successive pulses due to their finite width. The Number N_z of random coincidences is a function of the pulse width T_i and the number of impulses according to:

$$N_z = N_1 N_2 (T_1 + T_2), \tag{6.1}$$

where the counting rate of the PMTs are to be determined. This is done by determining the expected muon rate. A well known figure for astroparticle experimentalists is that of 1 muon/min/cm^2, this means that for the scintiallator area of 4000 cm^2, the PMT and discriminators should be set such as to register approximately 4000 counts/min. This is fufilled approximately when the total counting rate is about 6000 min^{-1}. The counting is done with a dedicated counter ("Scaler") which counts logical pulses for a user-selected period.

The number of random coincidences is thus expected to be:

$$N_z = \frac{6000^2}{60^2\,\mathrm{s}^2} 100 \times 10^{-9}\,\mathrm{s} \sim 1.0 \cdot 10^{-3}\,\mathrm{s}^{-1}, \tag{6.2}$$

which corresponds to ~ 0.06 events/min which is negligible when compared to the expected rate of 4000 events/min.

An expectation value for the effective count rate can then be computed: around 4000 muons are expected to cross the scintillator every minute, the efficiency of the setup is $\sim 50\%$, muons with energies between 601 and 617 MeV are stopped by the copper target. The energy spectrum shown in Figure 3.8 implies that about 4-5 events should be recorded every minute. This expectation is observed to be in good agreement with observations.

6.2 Electronic test with simulated pulse

A muon decay can be tested with the help of a pulse generator. The generator emits two short pulses with pre-set time intervals (which can be set from 10 ns to 1 s). The pulses must be passed

through discriminators 1 and 2, such as their time difference trigger the counter. If the distance is, per example 5 µs, the counter should display 100 (channels), one channel corresponding to 0.05 µs. If the double pulses are repeated frequently, the deviation shouldn't exceed ±1 channel. If there is a constant difference in the time interval ("offset"), this can be corrected later.

6.3 Expected time spectrum

In order to properly evaluate the data, proper knowledge of the muon decay counting rate N(t) is needed. Based on previous considerations, it is based on three components:

1. **The negative muon contribution** $N_{\mu^-}(t)$

   Muon decays are a statistical process obeying an exponential decay function given by:

   $$N_{\mu^-}(t) = N_- e^{\frac{-t}{\tau_-}}, \tag{6.3}$$

   with N_- a constant. A logarithmic representation should result in a straigth line for the graph. In a 12.5 µs window, it falls rapidely due to the limited lifetime of the negative muons which decay at 99% after 750 ns (see the stripped line in Figure 6.1).

2. **The positive muon contribution** $N_{\mu^+}(t)$

   The exponential decay for antimuons is slower because of their higher lifetime, the 99% decay mark is reached only after about 10 µs. Furthermore, the μ^+ in copper isn't bound the same way as the μ^- in the atom. Indeed, because of the precession, the emission direction will vary along with the Larmor Frequency ω_L and thus the probability of it being emitted towards the scintillator varies with the decay time. The spectrum from Equation 4.16 becomes:

   $$N_{\mu^+}(t) = N_+(1 + aP\cos\omega_L t + \Phi)e^{\frac{-t}{\tau_+}}, \tag{6.4}$$

   with N_+ a constant and $\omega_L t + \Phi$ the angle between the muon's spin and the detector (for a point-like detector). For an extended detector, an additional geometry factor G come in to play:

   $$N_{\mu^+}(t) = N_+(1 + aPG\cos\omega_L t + \Phi)e^{\frac{-t}{\tau_+}}, \tag{6.5}$$

   The geometry factor for an infinite detector, a reasonable enough assumption here, can be calculated as follows:

   $$N_{\mu^+}(t) \sim \frac{1}{\pi}\int_{\frac{-\pi}{2}}^{\frac{\pi}{2}}(1 + aP\cos\Theta d\Theta) = \ldots = 1 + aP\frac{2}{\pi}. \tag{6.6}$$

   The geometry factor is thus here about $G = \frac{2}{\pi} \simeq 0.64$. The infinite detector assumption representing the worst case, we in practice find the geometry factor to be $G = 0.68 \pm 0.04$, the expected asymmetry is then:

   $$A \doteq aPG = (0.38 \pm 0.04)\cdot(0.37 \pm 0.01)\cdot(0.68 \pm 0.04) = 0.096 \pm 0.019, \tag{6.7}$$

   which is between 7.5% and 11.5%. The proportion of positive muons is shown in Figure 6.1 with a greatly exagerated asymmetry.

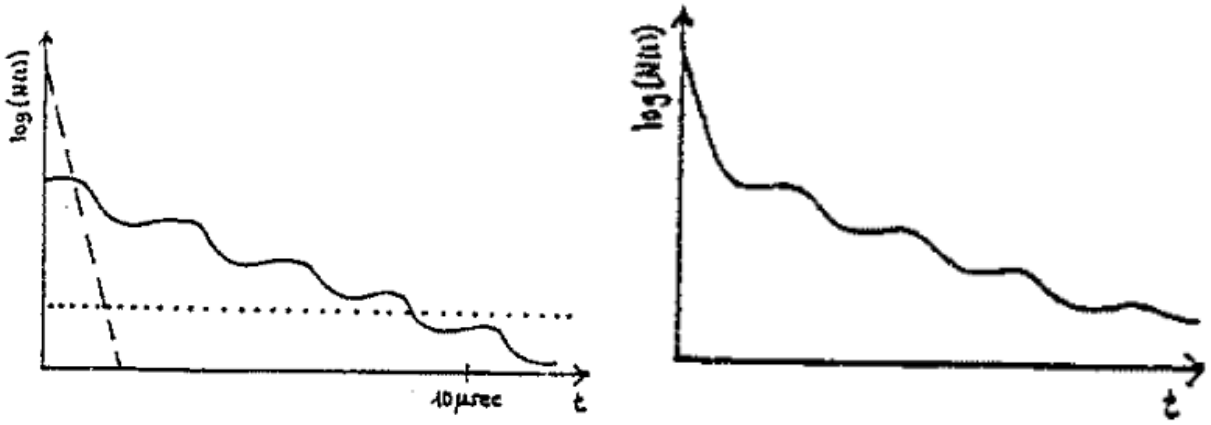

(a) (b)

Figure 6.1: (a) Components of the expected decay spectrum. The stripped line represents the negative muons, the solid line represents positive muons and the dotted line represents the constant background (b) Total decay (with greatly exagerated asymmetry).

3. **The background**

   Accidental coincidences contribute to create a constant background $N_{\mathrm{U}}(t) = U$.

   Thus, overall the following distribution is expected:

$$N(t) = N_{-}e^{\frac{-t}{\tau_{-}}} + N_{+}(1 + A\cos\omega_{\mathrm{L}}t + \Phi)e^{\frac{-t}{\tau_{+}}} + U. \tag{6.8}$$

   There are therefore eight parameters to consider: N_{-}, τ_{-}, N_{+}, τ_{+}, A, ω, Φ, U.

6.4 Analysis methods

Once the data has been acquired through the PC, it must be analyzed, this is done through fitting the parameters of the expected distribution to the data. Two ways to do so will be discussed here: the *optical fit* and the χ^2-minimization-based *SEEK* Algorithm.

6.4.1 Optical fit

The optical fit is, as it name suggests, a fit made by eye. The measured data points are displayed on a graph and one can then enter parameter values that are believed to well describe the distribution. Since estimating the cosine function form the μ^{+} decay spectrum is difficult, the asymmetry factor A is set to zero (as if no B-field was set) for optical fits. After recording the calibration of the TDC, it might be necessary to calibrate the data accordingly. For this purpose, the number of channels (each channel corresponds to 50 ns by which the measured data points need to be shifted (towards lower values) needs to be recorded in the time calibration field. This method has obvious faults: it's minimization is purely optical and thus quite unreliable, this is why one uses an automated χ^2 minimization fit.

6.4.2 χ^2 minimization fit

The χ^2 can be seen as a measure of the distance of data points to the expectation of the measurement and is defined by:

$$\chi^2 = \sum_{i=1}^{n} \frac{(O_i - E_i)^2}{E_i}, \tag{6.9}$$

where O is the observed data value and E is the expected data value for the given parameters. Given that data points are fixed, it is possible to vary the fitted function parameters and check the χ^2 at every step to ensure that it is being minimized. This can of course be done by hand, but effective minimization routines have been developed and are commonly used to perform such fits, minimizing parameters in succession to try to find the most effective set for a minimal χ^2. In order to judge the effectiveness of the fitting, a figure $\overline{\chi^2} = \frac{\chi^2}{N_{\text{df}}}$ is commonly used, with N_{df} the number of degrees of freedom. The number of degrees of freedom is defined by the number of independent sample points used to compute a statistic minus the number of parameters estimated from the sample points. A $\overline{\chi^2} \sim 1$ is the sign of a good fit, $\overline{\chi^2} < 1$, on the other hand, suggest overfitting: the overestimation of degrees of freedom.

One should also be careful not to let the fitting engine get stuck in a local minimum of the χ^2 distribution by using different starting values for the fit.

Popular χ^2 fitting engines in high energy physics are CERN ROOT's MINUIT algorithm [4] which can easily be used through a `TF1` fit or Python's scipy's `optimize.curve_fit` and `optimize.leastsq` which both make use of the Levenburg-Marquardt gradiant method [5].

Experiment schedule

6.5 On the day of the experiment

- Preliminary test: Elementary particles, cosmic rays, muon production, polarization and decay, experiment apparatus, decay spectrums.
- Setting up the electronics and PMT voltage, discriminators and gate lengths.
- Testing the electronics and calibrating the time measurement through simulated muons using the pulse generator.
- Starting the measurement.

The measurement lasts one week. The ensuing analysis is to be done at home, using whichever tools are seen fit. It is recommended that students review the functionning of the electronics, especially coincidence units and monoflops.

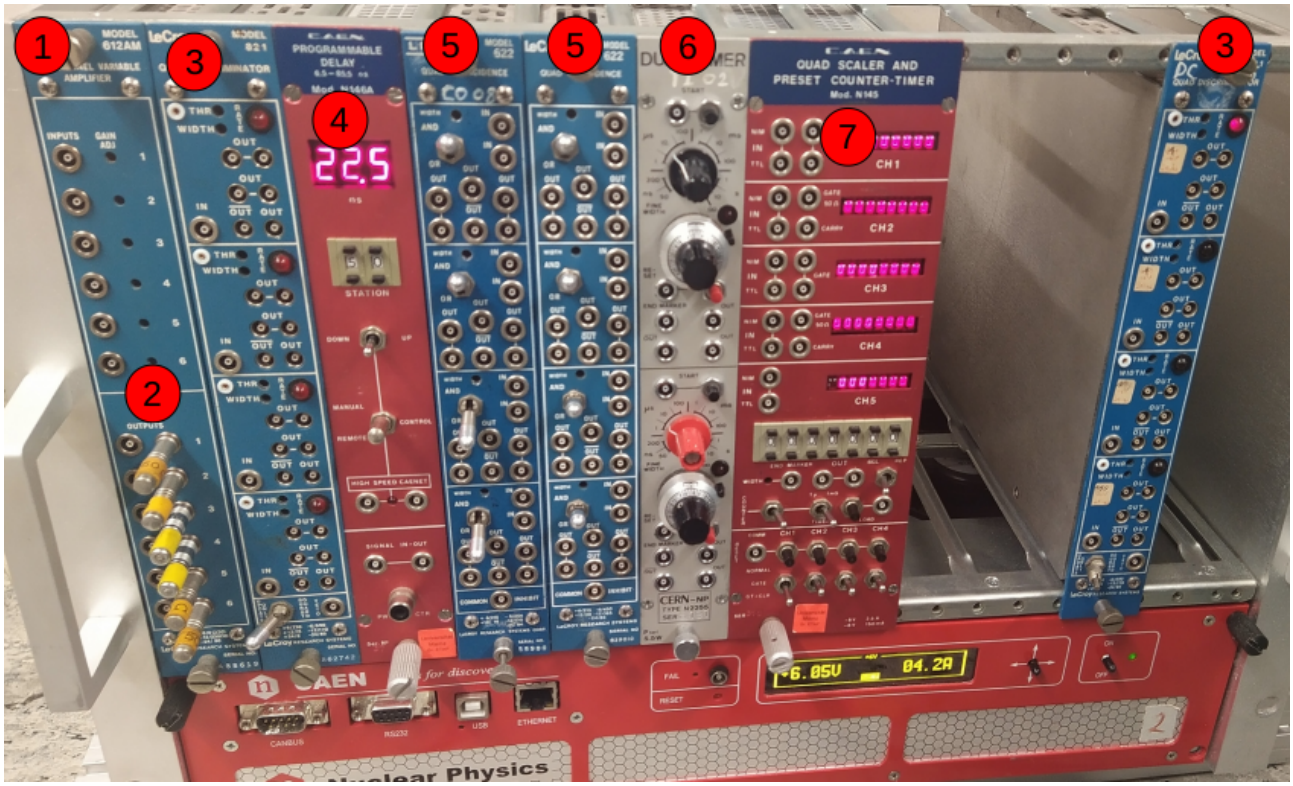

Figure 6.2: Picture of the electronic modules. (1) Amplifier input, the amplification can be tuned using a screwdriver in the holes left of the standerdized inputs. (2) Amplifier outputs. (3) Discriminators, parameters of the output gate can be tuned in the same way as the amplification for (1). (4) Programmable delay, the delay here is fixed at 22.5 ns. (5) Coincidence modules, they can be set to function in different ways (notably **AND** or **OR**). (6) Monoflop unit. (7) Digital counter, can be set to count over a period of time or to count "normally" (plug and count).

Annex

6.6 Electronics description

The different pieces of electronics used in this experiment are described here.

6.6.1 Amplifier

Amplifiers are an electronic device which is used to increase the amplitude of a signal through modulation of output voltage or current. The ratio between the output amplitude and the input amplitude is called the *Gain* (G). An example is shown in Figure 6.3

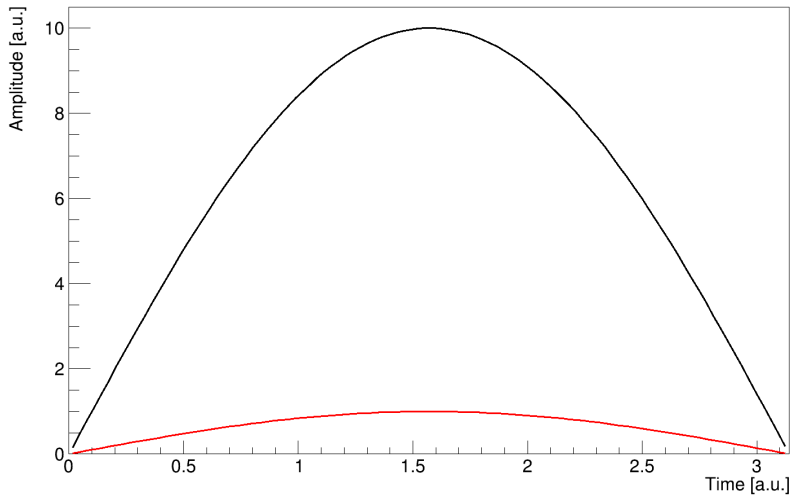

Figure 6.3: Signal wave (red) and its ten-fold ($G = 10$) amplified counterpart (black).

The experiment's amplifiers' gains can be tuned using a screwdriver on the holes left of the inputs.

6.6.2 Discriminators

Discriminators are an electronic Analog to Digital Converter (ADC). They produce a digital output when the signal fulfills certain conditions. If and when that is the case, a discriminator releases a single digital signal. Discriminators generally fall in one of two catergories: *Leading Edge Discriminators* or *Constant Fraction Discriminators* depending on which conditions they use to accept an analog signal:

- A leading edge discriminator only looks at the leading edge of signal, if the signal reaches the threshold level the logic pulse is emitted. This however can lead to *walk*: time variance dependent on the size of the signal. This can increase difficulty in adjusting the timing

information in the rest of the setup, and makes it impossible to obtain accurate timing information later. Thus, the constant fraction discriminator was created.

- A constant fraction discriminator (CFD) works by looking at the entire signal and emits the logical pulse when the input signal reaches a certain fraction of its peak value. In this way a signal that has a wide time variance can be narrowed significantly using a leading edge discriminator.

The rate in the experiment being low and the timing not being critical at this stage of the circuit, the discriminators used here are of LE type.

6.6.3 Monoflop unit

Monoflops (shortened for *Monostable Multivibrators*) are a sequential logic circuit that takes an input, two outputs and a clock unit (which may be seen as an extra input). The sequential part of the circuit (the clock) are continuous square function generators at a fixed frequency as shown in Figure

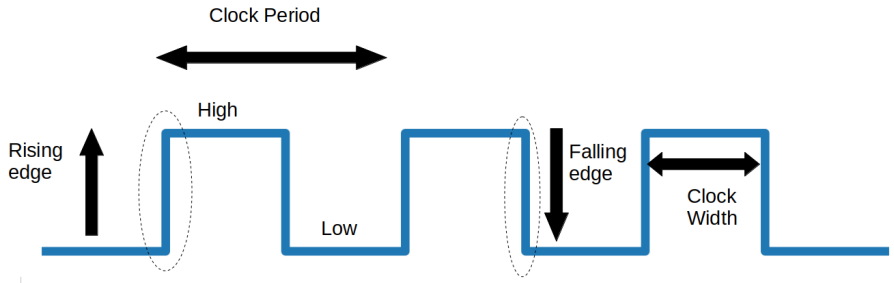

Figure 6.4: Clock parameters.

Such sequential logic circuits using clock signals for synchronization depend on their frequency and therefore the clock pulse width to activate their switching action. Sequential circuits can also change their switching state using either the rising edge, falling edge, or both edges of the clock signal.

Monostable Multivibrators or “one-shot” pulse generators are generally used to convert short, sharp pulses into much wider ones for timing applications. Monosflops generate a single output pulse, either 1 or 2, when a suitable external trigger signal or start pulse T is applied.

This trigger pulse signal initiates a timing cycle which causes the output of the monostable to change state at the start of the timing cycle, (t_1). The ouput remains in this second state until the end of the timing period, (t_2) which is determined by the time constant of its timing capacitor, CT and the resistor, RT.

The monostable multivibrator now stays in this second timing state until the end of the RC time constant and automatically “resets” or returns itself back to its original (stable) state.

In this experiment, the monoflop utilizes its clock to count over a set period of time, until it either received a second input (signaling a muon decay) or time runs out (no decay is seen/background).

Bibliography

[1] A. J. Dekker. *Secondary Electron Emission*, pages 418–445. Macmillan Education UK, London, 1981.

[2] M. Gardener, D. G. Jones, F. E. Taylor, and A. W. Wolfendale. The momentum spectrum of cosmic ray muons near sea level in the momentum range 0.4-10 GeV/c. *Proceedings of the Physical Society*, 80(3):697–709, sep 1962.

[3] M. Heel. Messung der lebensdauer und magnetisches moment von myonen aus der höhenstrahlung, 1992. University of Mainz.

[4] F. James.

[5] M. Lourakis. A brief description of the levenberg-marquardt algorithm implemened by levmar. *A Brief Description of the Levenberg-Marquardt Algorithm Implemented by Levmar*, 4, 01 2005.

[6] Qwerty123uiop. Wikipedia commons.

[7] L. T. Science. What are cosmic rays?, 2019.

[8] M. Tanabashi et al. Review of Particle Physics. *Phys. Rev. D*, 98(3):030001, 2018.